Journal of Energy Storage 57 (2023) 106274

Contents lists available at ScienceDirect

Journal of Energy Storage

journal homepage: www.elsevier.com/locate/est

Research papers

Energy management strategy for standalone DC microgrid system with photovoltaic/fuel cell/battery storage

Ramesh Gugulothu *, Bhookya Nagu, Deepak Pullaguram

Department of Electrical Engineering, National Institute of Technology Warangal, Telangana, India

ARTICLE INFO

Keywords:
DC microgrid
Energy management strategy (EMS)
Photovoltaic (PV) Array
Fuel cell (FC) system
Battery Bank

ABSTRACT

Standalone DC microgrids often have challenges in energy management for a long time horizon due to uncertain renewable energy sources and volatile loads. This paper presents a centralized energy management strategy (EMS) for a standalone DC microgrid with solar PV, fuel cells, and a battery energy storage system (BESS). The proposed EMS method is designed to improve the longevity of BESS, reliability, and reduce the hydrogen intake. In the proposed EMS, the PV system de-rating method is used to overcome the deep charging of battery under low-demand conditions. The fuel cell power supply is varied using a reverse sigmoidal function of the Batterys state of charge (SoC). This improves the hydrogen fuel efficiency and also helps in minimizing deep discharge of the battery under heavy loading conditions. The centralized EMS is fed with load power, battery SoC, and individual source power information. Consequently, the EMS provides decisive commands to the individual source local controller to control the respective output power. The efficacy of the proposed EMS under multiple operating conditions is evaluated in both simulation environment and on a hardware prototype of a DC microgrid.

1. Introduction

Increased focus on eco-friendly distributed generation has led to developments in microgrid systems, which provide additional reliability and flexibility over conventional power systems [1,2]. Microgrids are described as a cluster of distributed generation, energy storage devices, loads, and distribution networks. Microgrids can be operated in AC, DC, or AC-DC depending on the generation and load nature [3,4]. However, attention to DC microgrid is increasing as it has reduced conversion stages in generation (PV, Wind, fuel cells, Batteries, and load) and increased efficiency in DC load appliances (LED lighting, BLDC fans, and inverter-driven appliances like refrigerators, air conditioners). But any poorly managed standalone microgrid is always prone to reliability issues and increased operational costs. To achieve improved performance, reliability, and longevity of BESS, efficient energy management strategies (EMS) are required, which regulate power flow between sources and BESS to meet the load demand. These strategies may include a state machine approach, traditional proportional-integral (PI) control, fuzzy control, external energy optimization, equivalent minimization, and frequency decoupling authority [5].

1.1. Literature review

In a DC microgrid, power fluctuations are governed by three aspects [6]: power exchange variability, power variations in power sources and storage systems, and sudden changes in DC load. An efficient EMS is required to handle power fluctuations and provide energy balance for long-horizon [7]. An EMS for integrated PV battery Module is developed in [8,9] considering three possible architectures: AC-coupled, DC coupled, and inline architecture. For these architectures, seven operational modes are formulated and EMS is designed to control the system PV and battery power based on the operating mode. A coordinated strategy is designed for BESS, PV sources, and load management while considering battery state-of-charge (SoC) and battery power limitation [10], but a PV power regulation that might cause deep charging problems in BESS during standalone operation has not been considered. An intelligent EMS using a combination of fractional-order proportional-integral-derivative (FO-PID) and fuzzy logic controller methods was proposed for a hybrid wind/PV/battery-based DC-microgrid in [11]. In this, a fractional order PID is used for MPPT of renewable sources and fuzzy logic control(FLC) for tuning the gains of FO-PID. In [12], an EMS for power management in DC microgrid is developed using DC Bus Signaling (DBS), which uses bus voltage as a communication signal

* Corresponding author.
E-mail addresses: rameshphd@student.nitw.ac.in (R. Gugulothu), nagubhukya@nitw.ac.in (B. Nagu), drp@nitw.ac.in (D. Pullaguram).

https://doi.org/10.1016/j.est.2022.106274
Received 28 December 2021; Received in revised form 21 September 2022; Accepted 26 November 2022
Available online 5 December 2022

Nomenclature

PV	photovoltaic
SoC	state of charge
P_{H2max}	maximum safe pressure of the cylinder
P_{O_2}	oxygen gas pressure
V_{pv}	PV output voltage
P_{pv}	PV output power
D_{pv}^{old}	previous duty cycle of the PV
SoC_{min}	minimum limit of SoC
V_{dcref}	reference voltage signal
k_p	proportional controller gain
i_{fc}	fuel cell current
D_{bat}	battery duty cycle
P_{fcmax}	fuel cell maximum output power
EMS	energy management strategy
DGM	deficient generation mode
β	mid value of SoC limit
P_{bat}	battery output power
PEM	proton exchange Membrane
PM	phase margin
i_{Lbat}	bi-directional converter inductor current
d_{bat}	bidirectional converter change in duty
C_{bat}	bi-directional converter output capacitor
i_{load}	load current
$L_{io,\ cl}$	current loop gain of closed loop system
$G_{\Delta vdbat}$	duty to voltage control transfer function
BW	band width
HHV	higher heating value
BESS	battery energy storage system
P_{H_2}	hydrogen gas pressure
P_{H2min}	minimum hydrogen gas pressure
MPPT	maximum power point tracking
D_{pv}	PV duty cycle
P_{load}	load output power
SoC_{max}	maximum limit of SoC
V_{dc}	DC link voltage
i_{bat}^*	battery reference current
k_i	integral controller gain
i_{bat}	battery output current
P_{fc}^*	fuel cell power
P_{fcmin}	fuel cell minimum output power
EGM	excess generation mode
α	saturation constant
ΔV	change in voltage
MPP	maximum power point
BLDC	brushless DC electric motor
L_{bat}	bidirectional converter inductance
v_{bat}	bidirectional converter voltage
v_{cbat}	bidirectional converter capacitor voltage
D_{bat}	bidirectional converter duty
i_{pv}	PV current
$L_{io,\ op}$	current loop gain of open loop system
$L_{vo,\ op}$	voltage loop gain of open loop system
$G_{i_{bat}^* dbat}$	duty to current control transfer function
LED	light emitting diode
LHV	lower heating value

among the sources present in the microgrid. An EMS for PV/storage-based microgrid is presented in [13] using petri-nets modeling for each source, which is used to know the condition of each source. In energy management of a PV, batteries, and ultra capacitors are used for long-term energy supply and fast dynamic power regulation, respectively using Petri-nets modeling.

The presence of uncertain PV [14] and wind [15] sources, and the issue of power supply regulation between the fuel cell systems and storage systems is challenging and requires special attention while designing energy management strategies [16]. In [17,18], a multi objective optimization approach is developed to properly coordinate The seamless power supply for electric vehicles is provided by the battery, SC, and PEM fuel cells. However, the fuel cell is operated independently of the battery SoC. An energy management method for a photovoltaic system with BESS and fuel cells is proposed in [19], where a fuzzy logic controller (FLC) was used to maximize the PV power. The excess solar electricity is utilized to operate an electrolyzer to generate H2 and also to store the energy in BESS. However, the development of membership function are not detailed properly, and the system operation under extreme conditions such as extreme SoCs is not considered. Similarly in [20], a combined and dynamic rule-based power regulation of an off-grid solar/wind, and HESS consisting of a lithium-ion, a lead-acid battery, and a SC is developed. In [21], an energy management system for photovoltaic (PV) and wind power systems, along with battery storage is proposed so to fulfill the load requirements. A field-oriented control (FOC) technique of an induction motor (IM) powered by a PV system is used to manage the DC bus voltage. While both the sources are renewable, meeting the load requirements under all conditions might be challenging.

In DC microgrid, a voltage management technique with power balance limitation to minimize fuel exhaustion and increase performance is detailed in [22]. In [23], the functioning of the fuel cell is managed via an on-off switch threshold control technique based on the battery SOC. A predictive power management technique for switching the fuel cell and batteries based on predicted load demand and renewable energy source output power is proposed in [24]; However, the switching strategies might generate unnecessary transients in the microgrid. In [25], the authors presented an EMS for DC microgrid based on a multi-agent system implemented with Java Agent Development Framework (JADE), with PI controllers serving as EMS but this method is highly communication sensitive. Further, for PV–fuel cell–Battery–Super capacitor-based microgrid, an EMS using an adaptive fractional fuzzy sliding mode control (AFFSMC) technique is developed in [26].

Similarly, a model-based prediction control method was designed to maintain the voltage of DC bus and to restrict battery and fuel cell currents in [27,28]. In [29], an extremum seeking control scheme is developed in which the average power balancing is used to decrease the battery stack to a minimum level and efficiently operate the fuel cell stack. These energy management methods help to deal with power balancing challenges. Now a days, studies have been performed using a real hydrogen gas DC microgrid system. Due to technical restrictions, these methods are particularly very computationally intensive and place high demands on the computing performance of the controller. However, the EMS does not fully address the fuel cell's operational efficiency or the coordinated control of various control objectives. As fuel cells have greater generating cost than other forms of distributed generation, the efficiency has a significant impact on system efficiency and economics [30].

1.2. Features of proposed EMS and control

In this paper, an EMS for PV/fuel cell/ battery energy storage-based DC microgrid is developed to overcome existing challenges. This approach achieves the goals in a coordinated manner while regulating the fuel cell output power based on SOC and regulating hydrogen pressure and oxygen pressure while maintaining pres- sure difference

minimum to keep battery SoC within acceptable limits while ensuring efficient operation. The approach suggested classifies the complete system operation into nine possible operating states based on the battery bank's state of charge, the system's net demand power, and source output power. The following are the key contributions of the proposed standalone microgrid EMS:

- A de-rating strategy for a PV system is designed to effectively overcome the deep charging of batteries under light load conditions.
- The fuel cell power output power is controlled as a function of the battery's SoC to optimize the effective utilization of hydrogen fuel under light/medium loaded conditions and to minimize the deep discharge of the battery under heavily loaded conditions.
- A reverse sigmoidal function-based BESS SoC is used to provide smooth regulation of fuel cell output power.
- Real-time perturbations and operational conditions are considered in the hardware implementation of the proposed method.
- Improved reliability by adjusting the fuel cell hydrogen and oxygen pressures to enhance the fuel cell output power, and the FC is operated at the maximum power point (MPP) to satisfy the additional load demand.

The rest of the paper is organized as follows: Section 2 describes the DC microgrid and source levetron trolleys operation. The proposed energy management strategy is discussed in Section 3. Section 4 describes the Stability analysis of the proposed DC microgrid. The evaluation using simulations and different scenarios is detailed in Section 5 followed by experimental validation in Section 6. Finally, Section 7 concludes the paper.

2. System configurations and control

2.1. DC microgrid configuration

The Schematic representation of DC Microgrid with PV, fuel cell, and BESS is shown in Fig. 1. In this scheme, the PV and fuel cell are connected to the common DC-link through respective DC/DC boost converters while BESS is connected through a DC/DC bi-directional converter. The bi-directional converter enables the charging and discharging of BESS and it is designed to tackle power mismatch between the sources (PV, fuel cell) and the load. An EMS for PV, fuel cell, and BESS is developed to minimize sources and load power mismatch to ensure the longevity [31] of BESS and efficiently utilize hydrogen fuel. In the DC microgrid, the PV system is expected to operate either in MPPT or off MPPT (de-rated) based on BESS State of Charge (SoC) and load demand. The fuel cells output power is regulated based on battery SoC. As the fuel cell output power also depends on hydrogen and oxygen pressure, these pressure are increased to a limit while keeping the pressure difference minimum so to meet the additional load demand, (especially under peak load conditions). The output power of the solar PV systems, fuel cell, and BESS sources is controlled with their respective local controllers as per commands provided by the proposed EMS.

2.2. Solar PV local control

Solar PV systems [32–35] are usually expected to operate at MPP. However, in the standalone DC microgrid system, the PV system is expected to operate either in MPPT mode or off-MPPT (de-rated) mode, as commanded by the proposed EMS (discussed in Section 3). For MPPT operation, the conventional perturb-and-observe MPPT [36] shown in Fig. 3 is used to track the maximum power point by taking V_{pv} and I_{pv} as inputs, For off-MPPT mode, the operating point of the PV system is shifted to the right side of the MPP (as shown in Fig. 2) that curbs PV output power to meet energy balance requirements in the system. This is achieved by varying boost converter duty cycle (D_{pv}) using conditional logic (Eq. (1)).

$$D_{pv} = \begin{cases} D_{pv}^{old} + \Delta D_{pv}, & \text{if} P_{pv} - P_{load} < 0 \\ D_{pv}^{old} - \Delta D_{pv}, & \text{elseif } P_{pv} - P_{load} > 0 \\ D_{pv}^{old} & \text{otherwise} \end{cases} \quad (1)$$

Usually, under normal operating conditions, i.e., when$SoC < SoC_{max}$, the PV system is operated in MPPT mode by extracting maximum possible solar power. But, when$SoC \geq SoC_{max}$, the proposed EMS sends a

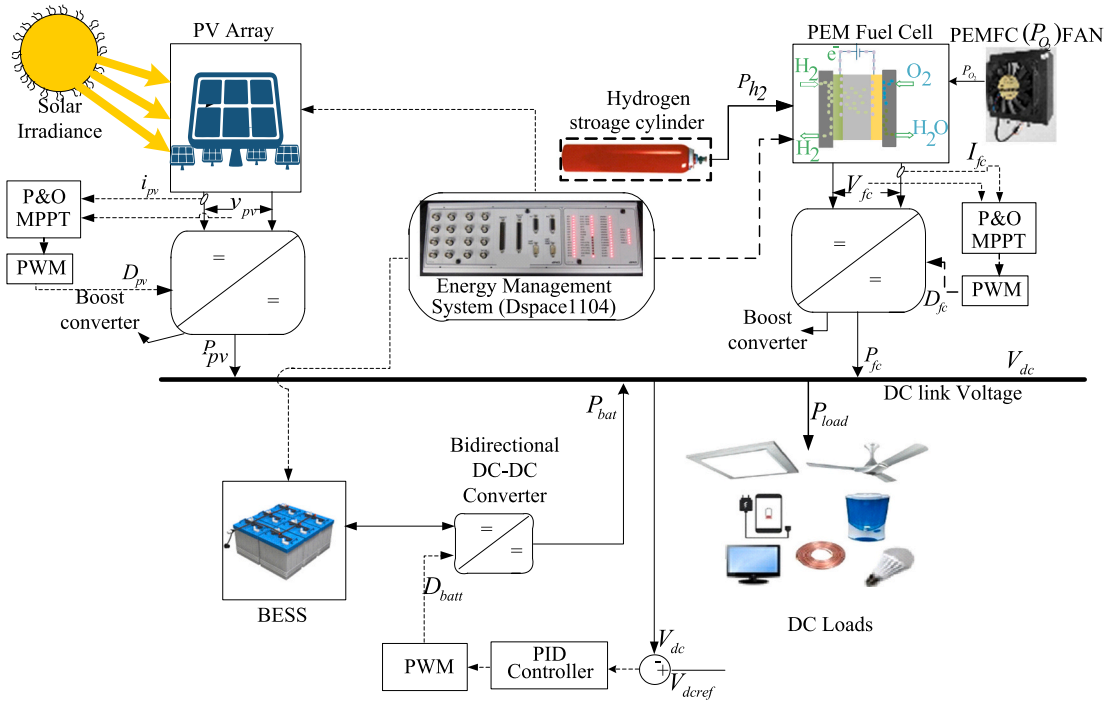

Fig. 1. Solar PV-fuel cell-battery standalone microgrid control and energy management strategy (EMS).

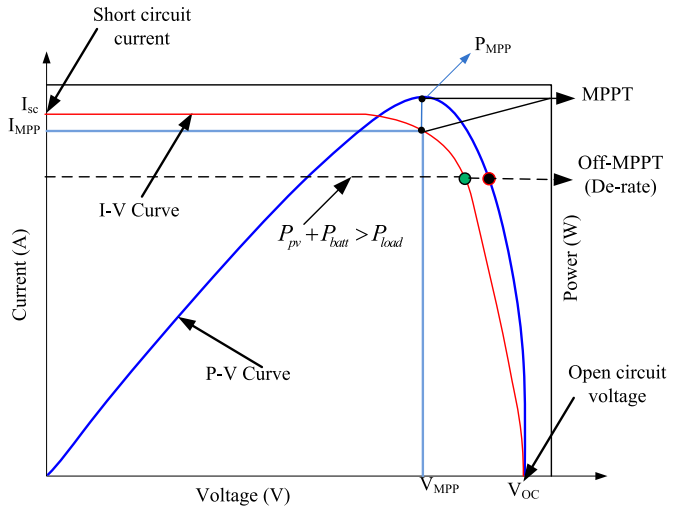

Fig. 2. Solar P-V and V-I characteristics.

status signal $S_{pv} = 0$ to PV controller indicating off-MPPT operation. Thus, the control now deviates from the MPPT and operates at reduced output power, which is equal to load power. Thereby avoids the deep charging of the battery. It is to be noted, during off-MPPT, the PV systems are operated on the right side of the MPP curve (as shown in Fig. 2) so to have a low deviation in PV voltage V_{pv}. This will support stable voltage operation in the microgrid.

2.3. Control technique of the proton exchange membrane fuel cell (PEMFC) model

2.3.1. PEMFC modeling

The complete fuel cell model has been developed and considers the auxiliary systems as shown in Fig. 4. Fuel cells are classified according to their electrolyte, operating temperature, electrodes, and use of costlier catalysts. The PEMFC was chosen for this work because of its low temperature operating range of 72 to 100°C, high output power densities of as much as 2W/cm^2, solid membranes, long cycle life, and because it has the most widely used form. The energy provided by a fuel cell is derived from the thermodynamic energy produced by its electrochemical processes within the cell. Essentially, this energy is derived by the exothermic process of water content from H_2 and O_2 [37].

$$H_2 + \frac{1}{2}O_2 = H_2O + Energy \tag{2}$$

This above energy is known as perhaps the enthalpy of structure $\Delta H = -285.84 kJ/mol$ (made reference to that as higher heating value (HHV)), and it may be categorized as the thermal energy, expressed by particular entropy $\Delta SkJ/mol.K$ calculated by multiplying by absolute

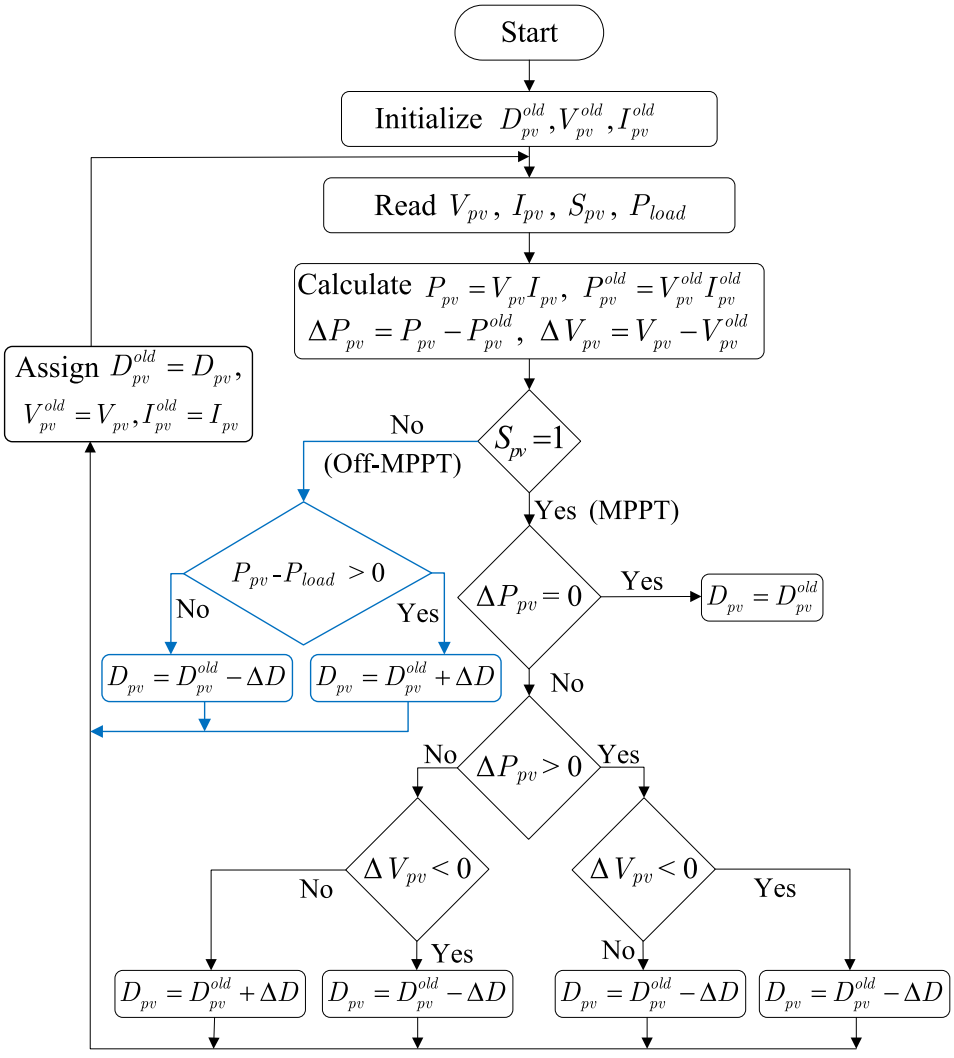

Fig. 3. Flow chart of P&O MPPT for PV System.

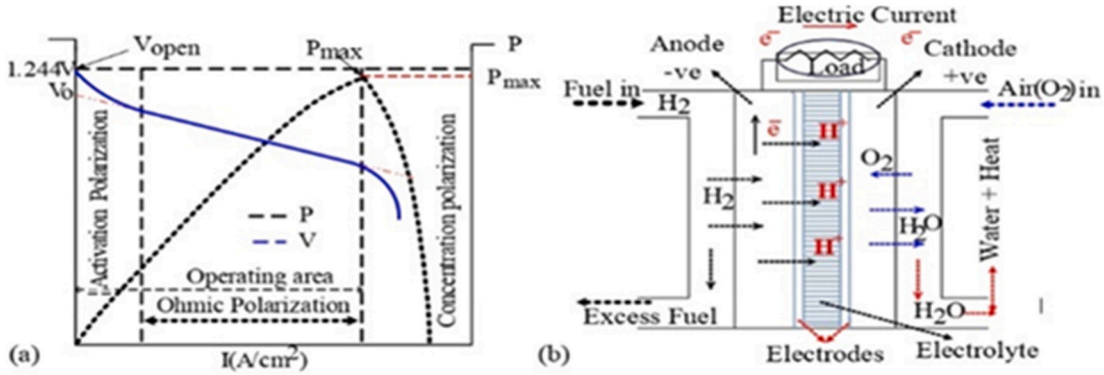

Fig. 4. Fuel cell (a) $P-I$ and $V-I$ characteristic (b) Functional diagram.

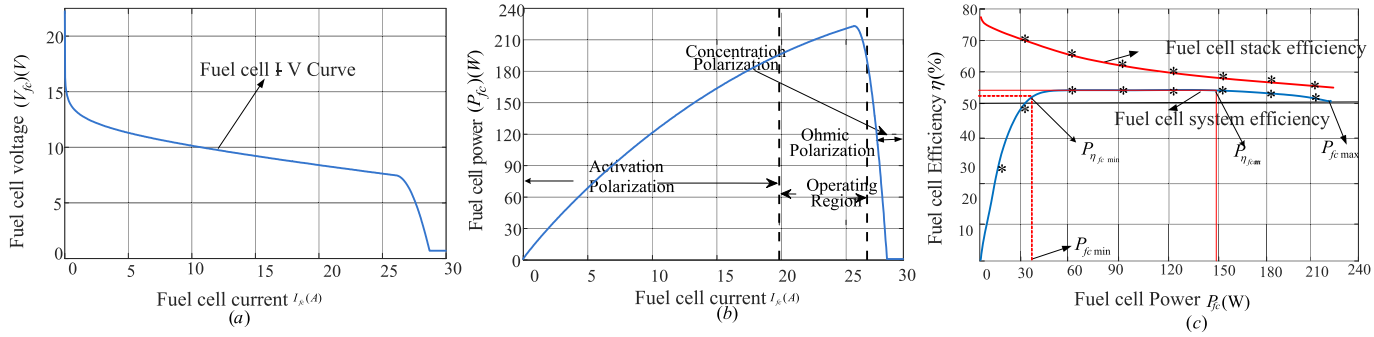

Fig. 5. I-V and I-P, and power- efficiency, curves of a fuel cell at constant hydrogen and oxygen gas pressure.

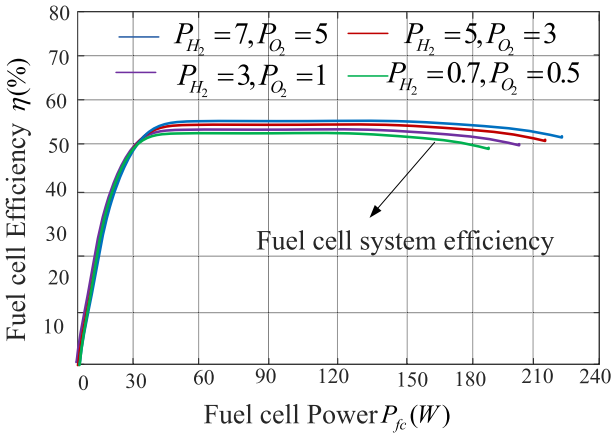

Fig. 6. Power- efficiency, curves of a fuel cell at various hydrogen and oxygen gas pressures.

temperature T, and productive work known as Gibbs free energies $\Delta GkJ/mol$, that can be exported as electricity, and yet ΔG is restricted by the second law of thermodynamics. As a result, the amount of energy is [37]:

$$\Delta H = \Delta G + T.\Delta S \tag{3}$$

where ΔG denotes the electrical work, which is described as the electrical charge Q [coulombs] from across the electrostatic potential $E[V]$:

$$\Delta G = -Q.E \tag{4}$$

Here Q has been the number of electron molecules (n), multiplied by (Faraday standard $F = 96485$ coulombs) for electron charge, then ΔG is as follows:

$$\Delta G = -n.F.E \tag{5}$$

Because the process is exothermic, the quantities of ΔG, ΔH, and ΔS become negative. As a result, the potential provided by the FC may be computed as follow

$$E = \frac{\Delta G}{n.F} = \frac{-(\Delta H - T.\Delta S)}{n.F} \tag{6}$$

This quantity must be changed to account for variations in temperatures and pressures of reactants relative to their rated values (T_{ref}= 25°, $P_{ref} = 1atm$). The consequence of temperature changes on potential is computed as follows, assuming that ΔH and ΔS remain consistent [37]:

$$\Delta E = \frac{\Delta G}{n.F}\left(T - T_{ref}\right) \tag{7}$$

From the above equation, the temperature rises, and the potential decreases since $\Delta S = -164J/mol.K$ is negative.

Now, variations in partial pressures impact ΔG, being a function of specific volumetric $V[m^3/mol]$ and density of pressure change $dP(asG = V.dP)$, and the final solution that describes this relationship (according to the universal fundamental gas law $V = R.T/P$) is:

$$\Delta G = \Delta G^{o} - \frac{R.T}{n.F}.Ln\frac{P_{O_2}^{0.5}.P_{H_2}^{1}}{P_{H_{2O}}^{1}} \tag{8}$$

In which $\Delta G^{o} = -237.17kJ/mol$ seems to be the Gibbs free energy during the standard test conditions, and $R = 8.3143J/mol.K$. This calculation assumes that perhaps the cell is operating on clean H_2 with partial pressure PH_2 as such fuel and clean O_2 with partial pressure PO_2 as such oxygen and that we know that one mole of water with pressure PH_{2O} (the product) requires one molecule of H_2, 1/2(half)a molecule of O_2 (i.e. reactants). As a result, the cell's potential is provided by [38]:

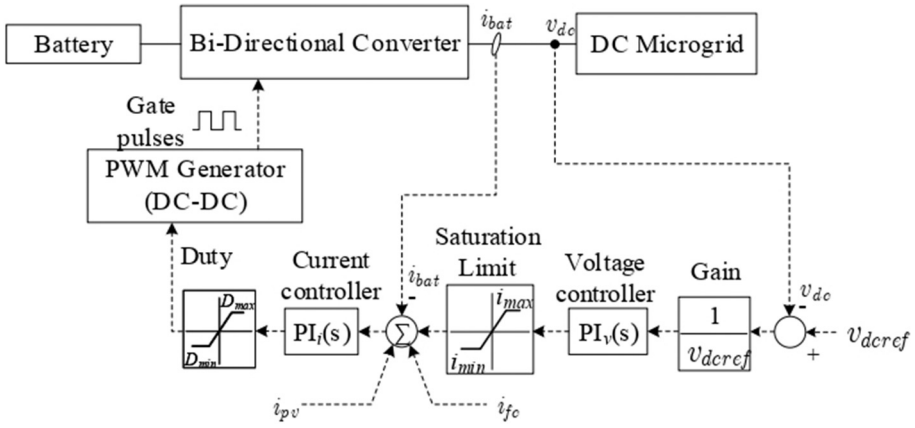

Fig. 7. DC-link voltage controller by using PI controller.

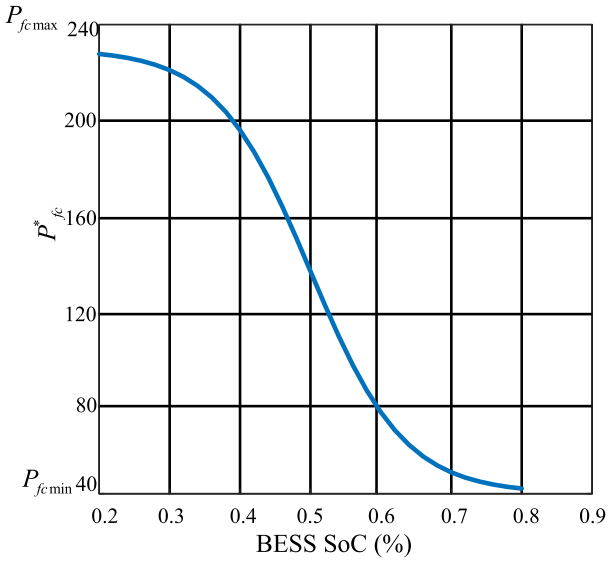

Fig. 8. Reverse sigmoidal function.

$$E_{Nerst} = \frac{\Delta G^o}{n.F} + \frac{\Delta S}{n.F}(T - T_{ref}) + \frac{R.T}{n.F}.ln\left(\frac{P^{0.5}_{O_2}.P^1_{H_2}}{P^1_{H_2O}}\right) \quad (9)$$

$$= 1.229 - 0.85*10^{-3}(T - 298.15) + 4.3085*10^{-5}*T*ln\left(P_{H_2}*\frac{P^{0.5}_{O_2}}{P^1_{H_2O}}\right) \quad (10)$$

This is known as the Nernst equation. This refers to the highest voltage that the FC can provide owing to losses including overpotentials, which have been divided into four distinct types:

2.3.2. The activation loss

The above loss is recognized as the igniting spark required initiating the reactions. It is determined using a semi-empirical equation that takes into account the partial pressures (PH_2, PO_2), temperature (T), and the activator employed on the counter electrode: [39] The activation voltage dropV_{act} is given as [40]

$$V_{act} = [\xi_1 + \xi_2 T + \xi_3 Tln(C_{O_2}) + \xi_4 Tln(I_{FC})] \quad (11)$$

where $\xi_i(i = 1 - 4)$ represent the FC properties coefficients, CO_2 (atm) represents the oxygen content in (mol cm^{-3}) provided by Eq. (10), and I_{FC} represents the FC current.

$$CO_2 = \frac{P_{O_2}}{(5.08 \times 10^6) \times exp(-498/T)} \quad (12)$$

2.3.3. The ohmic loss

V_{ohmic} is The ohmic-voltage drop was calculated as follows:

$$V_{ohmic} = I_{FC}(R_M + R_C) \quad (13)$$

The Vohmic of the cell can be reduced by employing conductive substances as well as an electrolyte barrier. RC in Eq. (13) is the edge

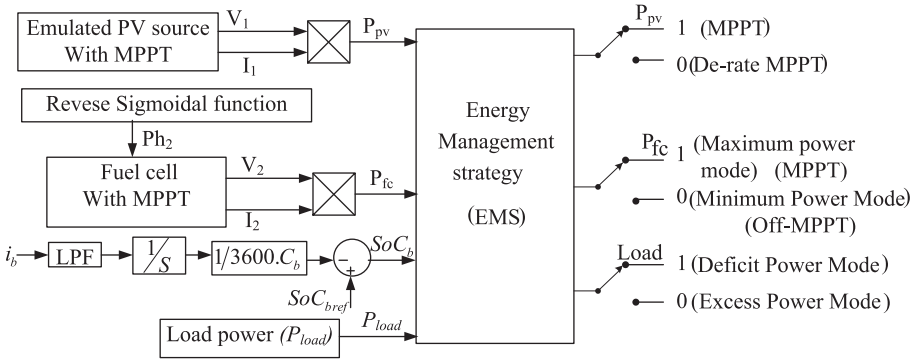

Fig. 9. Proposed system for energy management.

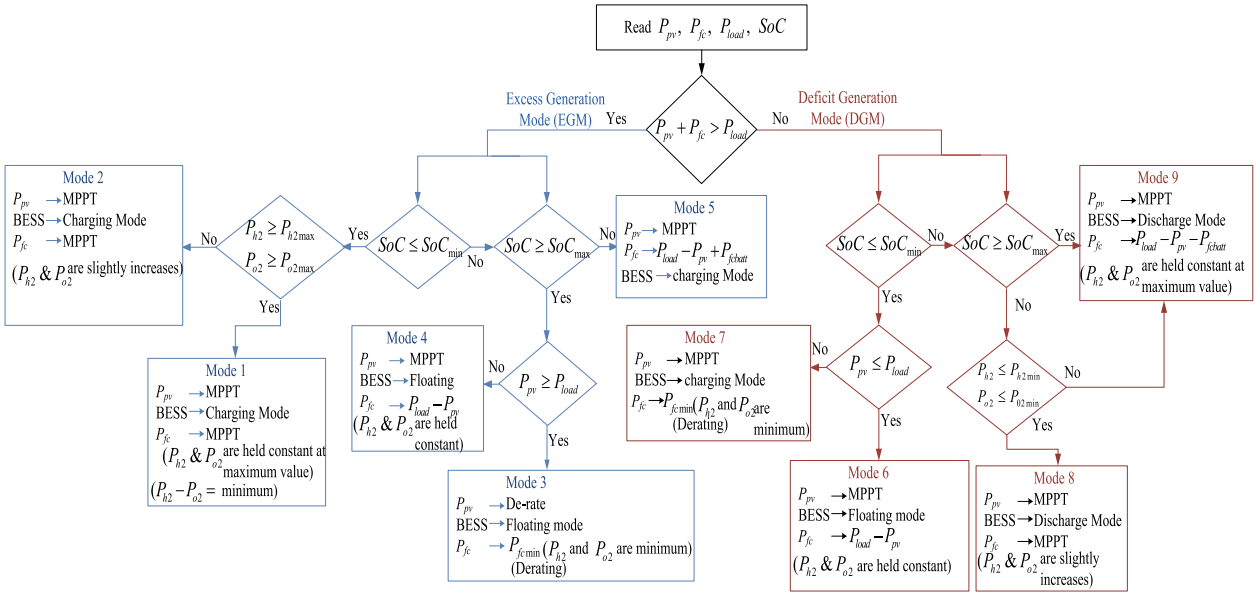

Fig. 10. Flowchart for modes of operation in PV, fuel cell and BESS system with proposed energy management strategy.

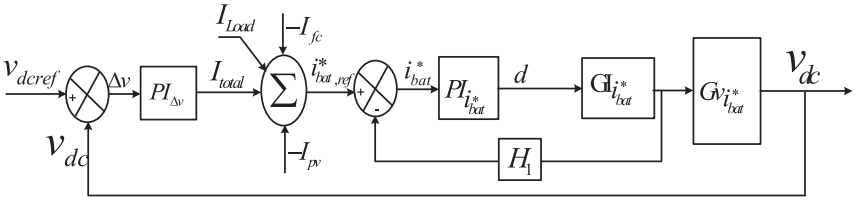

Fig. 11. Stability analysis of feedforward loop system.

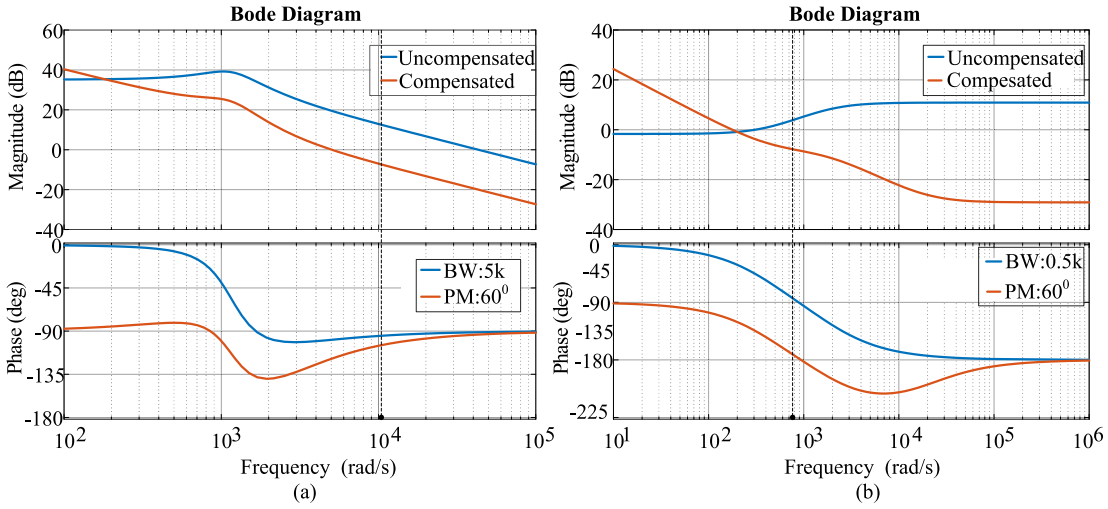

Fig. 12. Bode plot for (a) current control loop, (b) voltage control loop.

contact resistance, which would be considered to be constant because it is independent of FC operating temperature. RM seems to be the PEM's resistance, which is given by an empirical formula.

$$R_M = \frac{r_m t_m}{A} \tag{14}$$

$$r_m = \frac{181.6\left[1+0.03\left(\frac{I_{FC}}{A}\right)+0.0062\left(\frac{T}{303}\right)^2\left(\frac{I_{FC}}{A}\right)^{2.5}\right]}{\left[\lambda_m-0.634-3\left(\frac{I_{FC}}{A}\right)\right]exp\left[\left(4.18\left(T-\frac{303}{T}\right)\right)\right]} \tag{15}$$

Here r_m is the electrolyte barrier resistance in (Ω. cm), t_m = (0.0178cm) is the thickness of the barrier, A = 232 (cm^2) is the functional region of the FC, and,λ_m is barrier water content with a normal value range of (0to14) and relative humidity of 100%.

2.3.4. *The concentration loss*

The voltage loss (V_{con}) caused by overflowing of water inside the FC substances [41]:

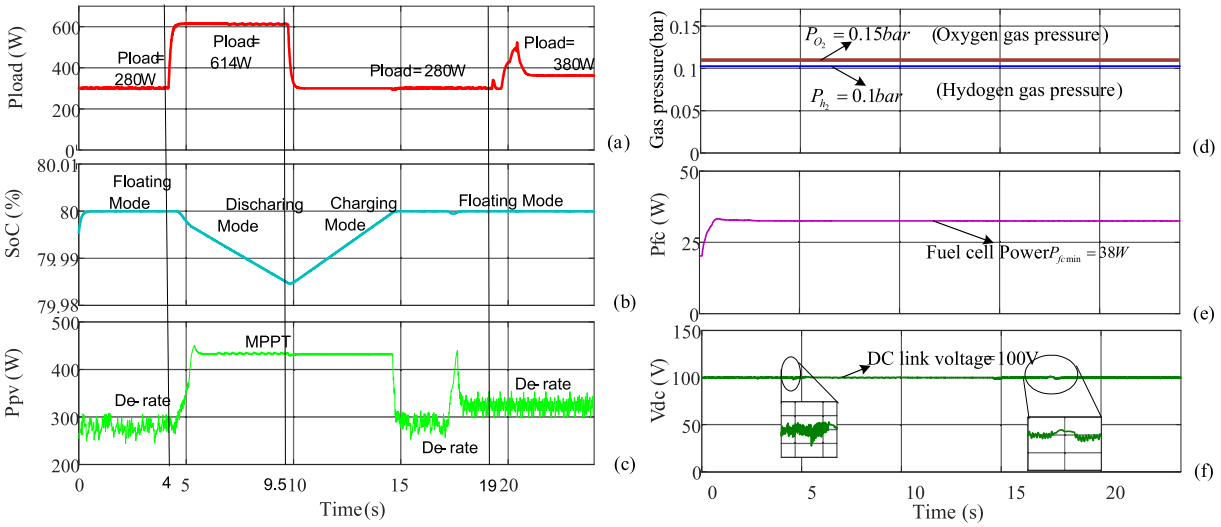

Fig. 13. BESS SoC = 80% with load changes (a) Load power (Pload) (b) Battery SoC(%) (c) PV power (Ppv) (d) Hydrogen pressure (Ph2), and Oxygen gas pressure (Po2) (e) Fuel cell power (Pfc) (f) DC link voltage (Vdc)

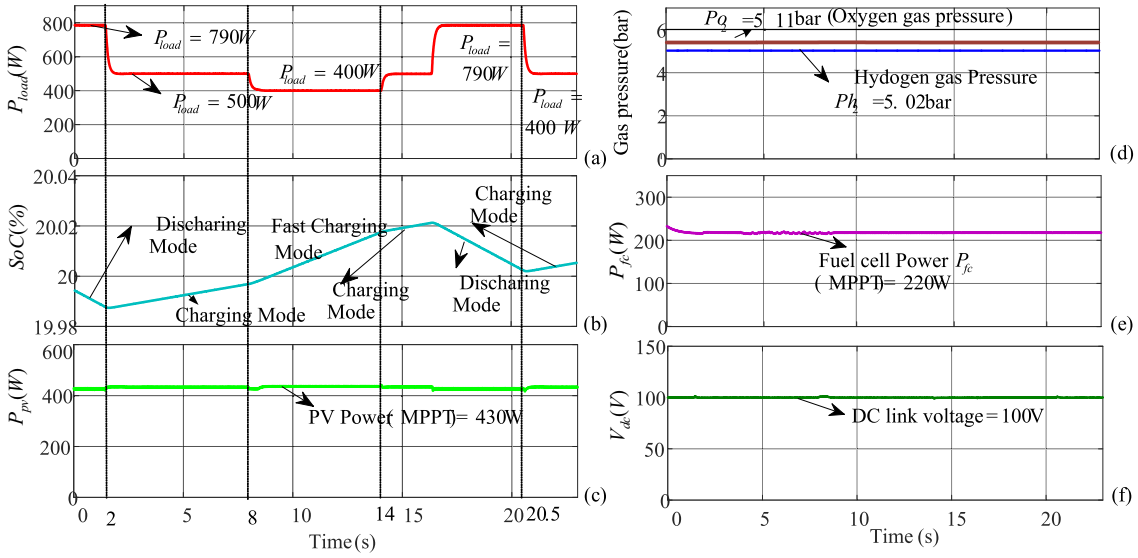

Fig. 14. BESS SoC = 20% with load changes (a) Load power (Pload) (b) Battery SoC(%) (c) PV power (Ppv) (d) Hydrogen pressure (Ph2), and Oxygen gas pressure (Po2) (e) Fuel cell power (Pfc) (f) DC link voltage (Vdc).

$$V_{Con} = -\frac{RT}{nF} * ln\left(1 - \frac{I_{FC}}{i_L A}\right) \tag{16}$$

where n denotes the number of electrons moving towards the reactions, i_L denotes the limitation current, and R denotes the gaseous universal constant.

2.3.5. The cross over loss

The partial pressure of (PH_2, PO_2), temperature (T), and barrier water content (λ_m) all impact the FC stack voltage. Furthermore, the FC voltage exhibits drooping V-I characterization due to a drop in voltage caused by activation, concentration, and ohmic losses. Taking these drops into account, the FC dc voltage is signified as [42].

$$V_{cell} = E_{Nernst} - V_{act} - V_{ohmic} - V_{con} \tag{17}$$

The total output voltages and power of said stacked FC were calculated as follows:

$$V_{FC} = N_{FC} V_{cell} \tag{18}$$

$$P_{FC} = V_{FC} I_{FC} \tag{19}$$

where, (N_{FC} = 35) represents the number of FCs, (V_{FC}), (I_{FC}), and (P_{FC}) represents the output power, voltage, and current of the FC stack, respectively.

2.3.6. Stack efficiency

The equation may be used to calculate the FC efficiency [43].

$$\eta = \mu f . \frac{V_{FC}}{1.48} \tag{20}$$

where μf is the fuel utilization coefficient, which is typically within 95% of the range, and 1.48 V indicates the highest voltage attained by employing the higher heating value (HHV) for every hydrogen pressure enthalpy. In a fuel cell has a hydrogen pressure flow rate controller, fuel usage is kept constant. In this situation, hydrogen is given based on the load current.

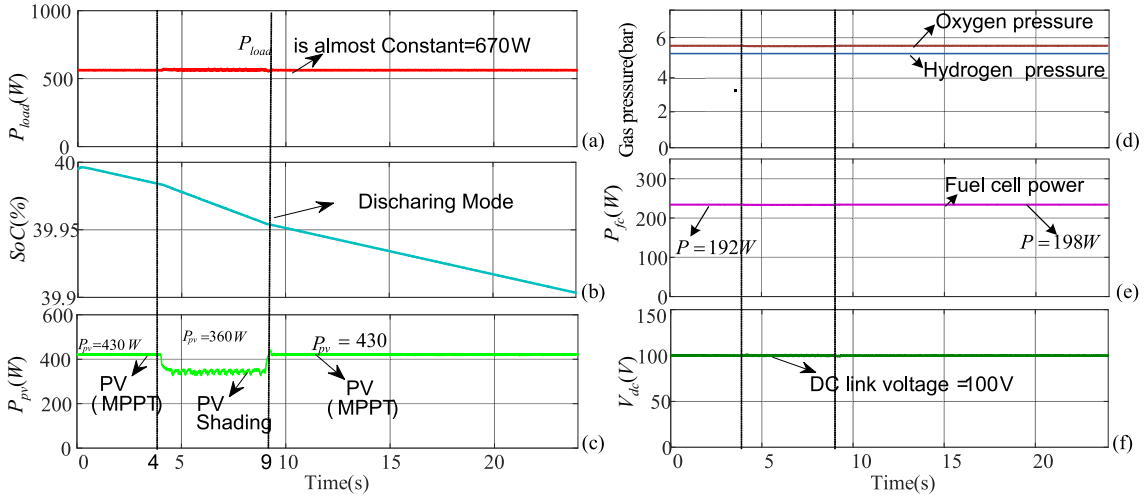

Fig. 15. Minimum BESS SoC = 40% with PV Shaded Condition (a) Load power (Pload) (b) Battery SoC(%)(c) PV power (Ppv) (d) Hydrogen pressure (Ph2),and Oxygen gas pressure (Po2) (e) Fuel cell power (Pfc) (f) DC link voltage (Vdc).

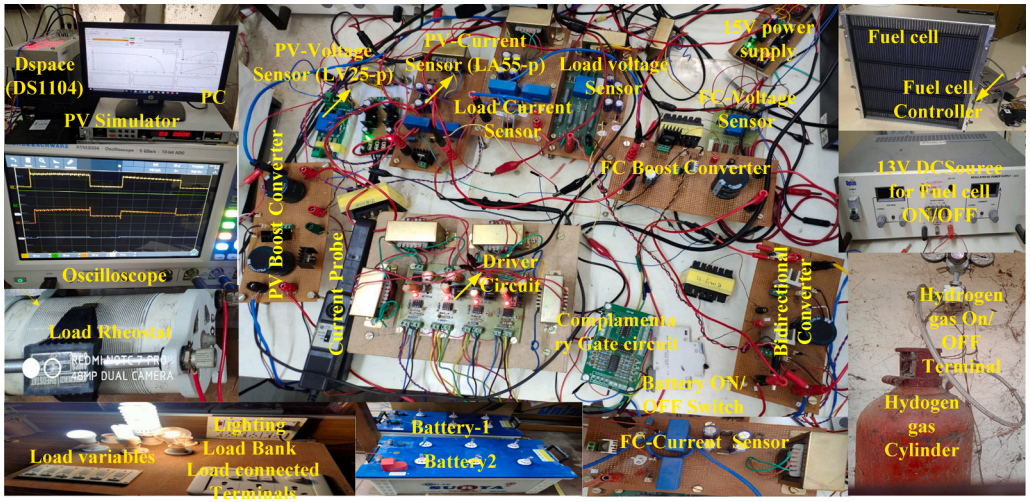

Fig. 16. Experimental setup.

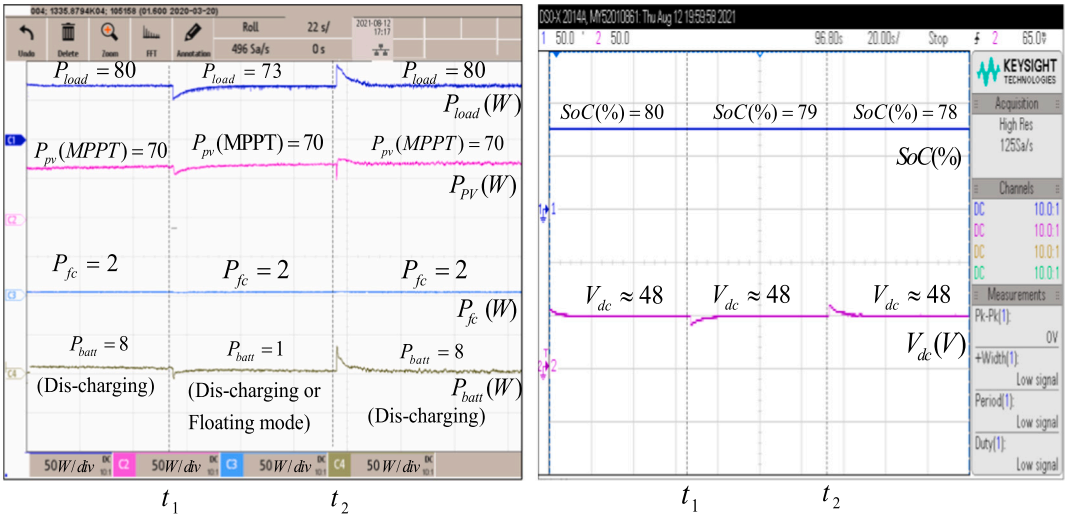

Fig. 17. BESS SoC = 80 % with load changes, (a) Load power (Pload), PV power (Ppv), Fuel cell power (Pfc), (b) Battery SoC (%), DC link Voltage (Vdc).

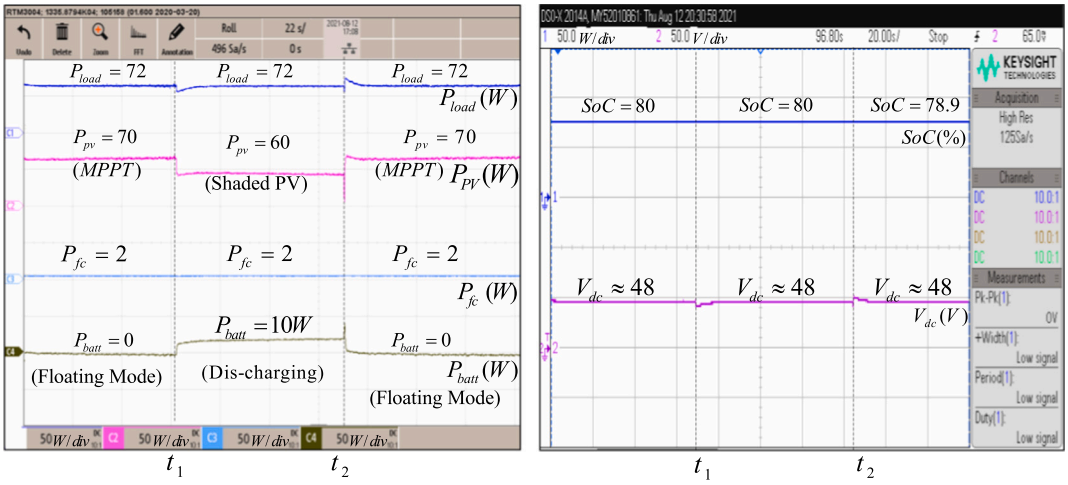

Fig. 18. BESS SoC = 80 % with PV shaded Condition (a) Load power (Pload), PV power (Ppv), Fuel cell power (Pfc), (b) Battery SoC (%), DC link Voltage (Vdc).

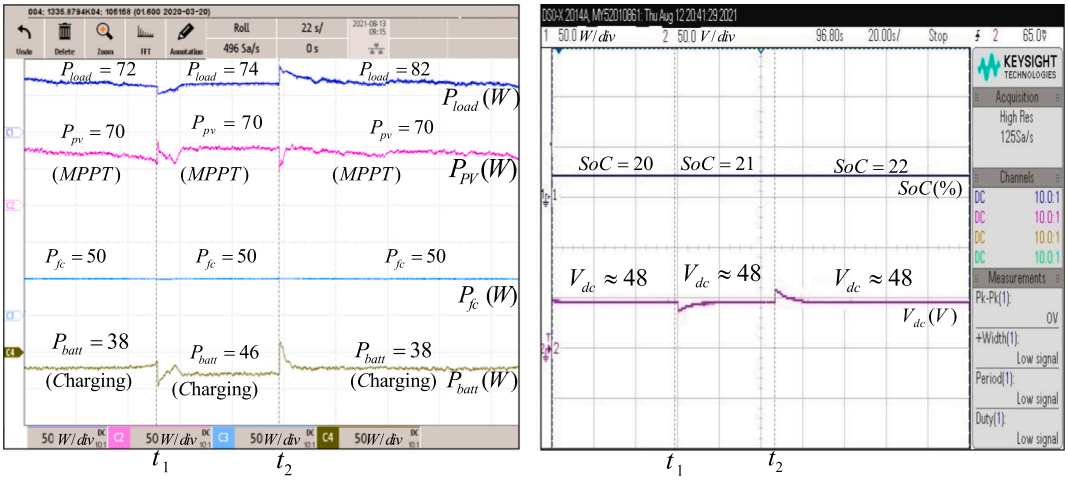

Fig. 19. BESS SoC = 20 % with load changes (a) Load power (Pload), PV power (Ppv), Fuel cell power (Pfc), (b) Battery SoC (%), DC link Voltage (Vdc).

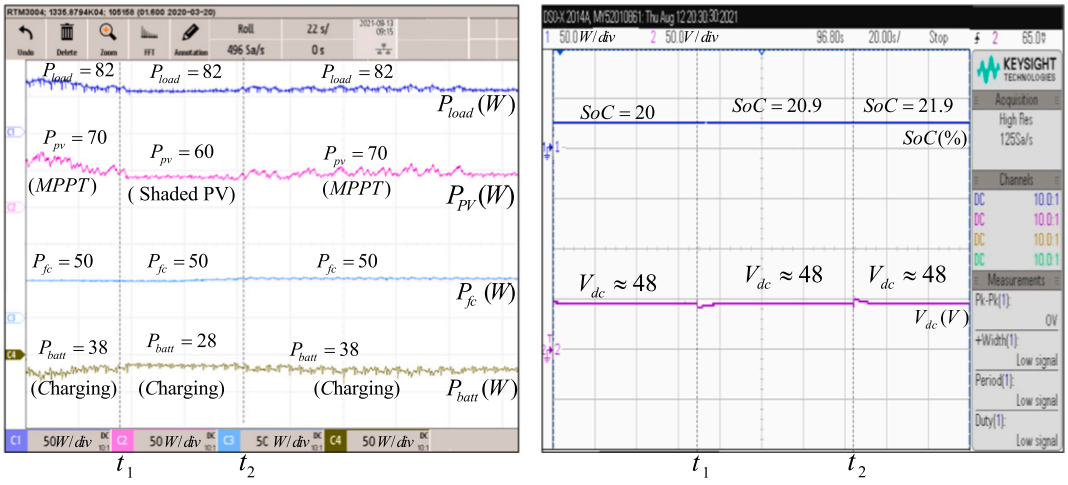

Fig. 20. BESS SoC = 20 % with PV shaded condition (a) Load power (Pload), PV power (Ppv), Fuel cell power (Pfc), (b) Battery SoC (%), DC link Voltage (Vdc).

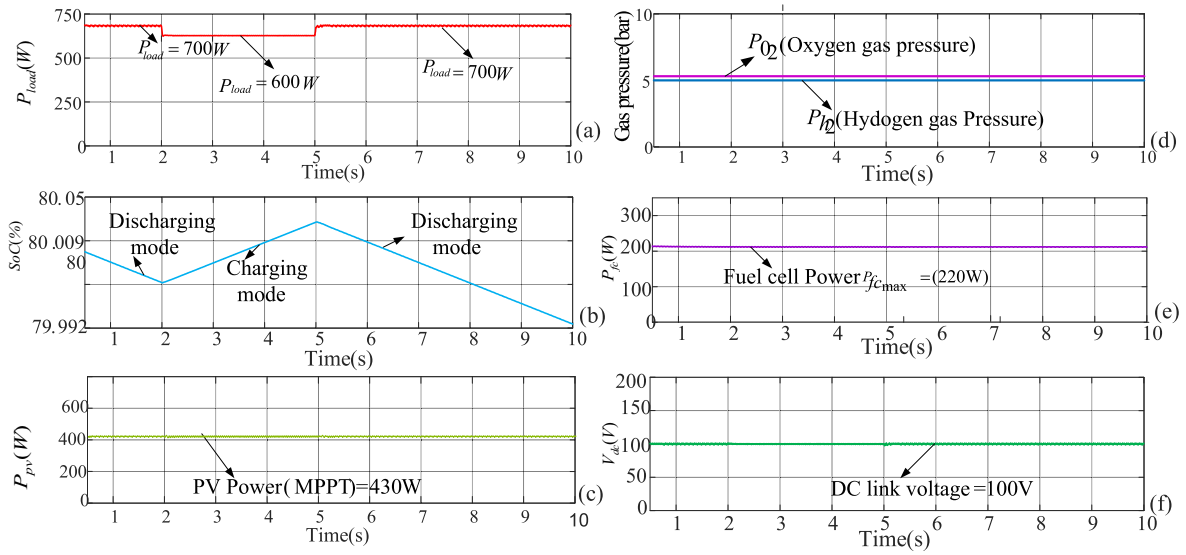

Fig. 21. BESS SoC = 80%, load changes without EMS (a) Load power (Pload) (b) Battery SoC(%) (c) PV power (Ppv) (d) Hydrogen pressure (Ph2), and Oxygen gas pressure (Po2) (e) Fuel cell power (Pfc) (f) DC link voltage (Vdc).

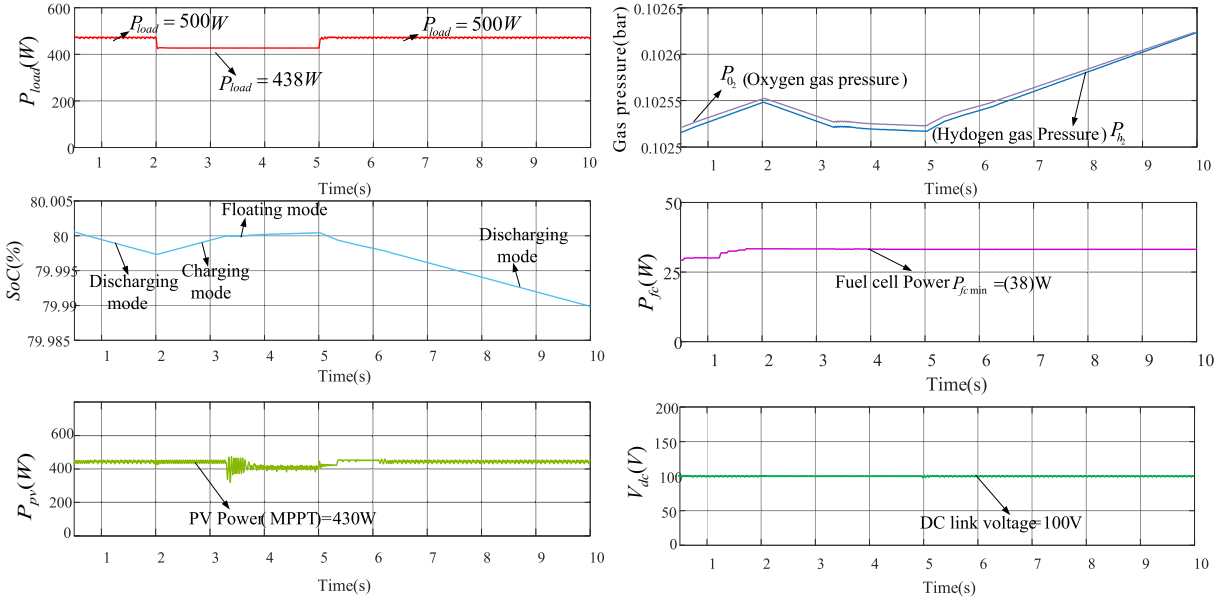

Fig. 22. BESS SoC = 80%, load changes with proposed EMS (a) Load power (Pload) (b) Battery SoC(%)(c) PV power (Ppv) (d) Hydrogen pressure (Ph2), and Oxygen gas pressure (Po2) (e) Fuel cell power (Pfc) (f) DC link voltage (Vdc).

2.3.7. *Calculating fuel cell system efficiency (η_{FCS})*

The standard method for calculating the efficiency of a fuel cell power plant or other electrical generation device is to divide the net electricity generated by the higher heating value (HHV) of the fuel used [44] i.e.,

$$\text{Electrical Efficiency} = \frac{Electricity\ generated}{HHV\ of\ fuel\ used} \tag{21}$$

This is a reasonable method for calculating power plant efficiency because the power-plant operator purchases fuel (natural gas is sold by heating value) and sells electricity. However, the maximum theoretical limit to the electrical efficiency of a fuel cell system is represented by using the Gibbs free energy divided by the combustion heat of the fuel. In the case of the hydrogen fuel cell, this value is the Gibbs free energy/HHV (237.2*kJ/mole* / 285.8*kJ/mole* = 83%). The use of HHV here is in keeping with the method used in the United States to calculate efficiency for internal combustion (IC) engine/generators and gas turbine/generator systems [45]. Some U.S. developers of high-temperature fuel cells, however, prefer the European convention and instead use the lower heating value (LHV) of hydrogen for efficiency calculations. The Joint Army-Navy-Air PForce (JANAF) Tables list the Gibbs free energy for the formation of water vapor from hydrogen and oxygen as 228.6*kJ/mole*, so the maximum theoretical efficiency of a complete fuel cell system based on the LHV of hydrogen is 228.6*kJ/mole*241.8*kJ/mole*, *or* 94.5 % . Using the LHV convention for calculating the efficiency of an electrical generator always yields numbers greater than those yielded by calculations using the HHV for the same system. When quoting the electrical efficiency of an electric generator, it is important to indicate whether it is based on the HHV or the LHV calculation method.

Practical fuel cells cannot achieve these maximum electrical efficiency values due to the presence of internal resistance losses and other losses. The practically calculated fuel cell efficiency using the number

(Eq. (20)) for varying output power is shown in Fig. 5(b).

A practical fuel cell operating near its maximum power output might be able to produce only 154 kJ of electricity per mole of hydrogen consumed, with the rest of the heating value appearing as heat produced by the fuel cell. The calculation for such a fuel cell is 154 kJ/mol 285.8 kJ/mol efficient (HHV). However, the remaining 46% of the energy produced can be recovered from the fuel cell system as co-generated heat [44,46].

As it is observed from Fig. 5(c). The fuel cell system efficiency is very low for the low value of output power and it is sharply increased with the increase in output power, up to a value of P_{fcmin}. Beyond this output power, although the rate of increase in efficiency with output power is positive, it is very small in magnitude. In this curve, the peak efficiency value ($P_{\eta fcmax}$) is observed when the fuel cells system output power is P_{fcmax}. On the further increase of output power, the efficiency is reduced with a small negative slope magnitude. From these efficiency characteristics, it can be observed that fuel cell system efficiency is merely constant when the output power of the system is between P_{fcmin}. and P_{fcmin}. Even at the MPP point, the efficiency is observed to be 7% lower than its peak value. Thus, taking this advantage the proposed strategy can be easily employed by maintaining the fuel cell minimum power, i.e. P_{fcmin}. (or power corresponding to the nose point in the efficiency curve), when batteries are overcharged and power balance is achieved by derating PV. During normal operation, the fuel cell is operating using a reverse sigmoidal function, delivering power between P_{fcmin} to P_{fcmax}. The reverse sigmoidal characteristics are modified accordingly to fit within the output power limits with in these ranges. Further, the different efficiency curves under different operating pressures of hydrogen and oxygen are also shown in Fig. 6.

2.4. DC-link voltage controller by using BESS

In BESS, a bi-directional DC/DC converter is employed to regulate common DC-link voltage. As BESS is regulating DC-link voltage, any power imbalance between sources and load demand is taken care of by BESS. The conventional cascaded voltage and current controller scheme [2] is adopted for BESS as shown in Fig. 7. The measured dc-link voltage (v_{dc}) is compared with a reference voltage signal (v_{dcref}) and fed to a PI-based voltage controller. The output of the controller is considered battery reference current (i_{bat}*) and given in Eqs (22) and (23):

$$\Delta v(t) = V_{dcref(t)} - V_{dc(t)} \tag{22}$$

$$i^{*}_{bat}(t) = k_p \Delta v(t) + k_i \int \Delta v(t)dt - i_{pv}(t) - i_{fc}(t) \tag{23}$$

Here k_p and k_i are the gains of voltage PI controller.

The battery reference current is limited using the saturation limits to avoid any prolonged over-current that can damage BESS converter switches. The battery current (i_{bat}) measured is then compared with reference current signal (i_{bat}*) obtained and fed to inner current PI controller which in turn provides duty-cycle (D_{bat}) as output. A PWM generator is used to generate the switching pulses that trigger bidirectional converter as per the duty cycle (D_{bat}) obtained from the controller, as shown in Fig. 7.

2.4.1. Designing of BESS controller

For the PI regulator of the battery, voltage controller dynamics is very slow compared to current controller dynamics, and switching frequency ($f_{sw} = 20KHz$).The current controller gains are calculated based on the filter inductor inductance (L_f) and resistance (R_f) and converter switching frequency (f_{sw}). First, the current controller is designed to have a bandwidth slower than the switching frequency.

Thus, the current controller time constant T_c is chosen such that it is greater than the settling time of switching frequency, i.e.,

$$T_c = \frac{10}{2*\Pi*f_{sw}}; \tag{24}$$

The proportional (K_{pc}) and integral controller (K_{ic}) gains of the current controller are calculated using the pole zero cancellation approach. The zero of the PI controller ($K_{pc}s + K_{ic}$) should cancel the pole of the system due to the series filter ($\frac{1}{L_f s + R_f}$). Thus

$$K_{pc} = \frac{L_f}{T_c} \tag{25}$$

where, L_f= inductance value (henry)

$$K_{ic} = \frac{R_f}{T_c} \tag{26}$$

where, R_f = inductor resistance (ohms). Similarly, the voltage controller is designed with a lower bandwidth than the current controller. Let T_v the time constant of the voltage controller be greater than the settling time of the current controller. $T_v = 5$ to 10 times of T_c (settling time of T_c) Now the proportional (K_{pv}) and integral (K_{iv}) gains of the voltage controller are calculated by fixing one of the gains to a constant and having a time constant T_v. Thus assuming the $K_{iv} = 50$, the K_{pv} is calculated as

$$K_{pv} = T_v * K_{iv} \tag{27}$$

It needs to be noted that if i_{bat}* is positive while Δv is positive, the input power to the dc-link is greater than that of the output power, and vice versa. Thus the DC-link voltage is raised (or reduced) to make the net power imbalance and voltage deviation across the DC-link zero. Typically, when the load demand is high, and the battery SoC is greater than battery SoC_{min} the bidirectional converter operates as in boost mode (discharging mode) supply when using power from the battery. When load demand is low, and battery SoC is less than the upper limit, the battery operates in buck mode (charging mode or floating mode).

3. Energy management strategy (EMS)

In this paper, to efficiently utilize sources (PV, fuel cell, and BESS) for supplying load demand, to improve longevity, and to ensure minimum consumption of hydrogen, an EMS scheme has been proposed. Here, a rule-based controller scheme is implemented for EMS by considering load (P_{load}) and battery SoC level. The proposed system for EMS is shown in Fig. 9. In EMS, Battery SoC is monitored and the operating points for all the sources are calculated to maintain SoC within limits while regulating the DC-link voltage at nominal value. In all operating conditions, S_{pv} represents PV status that is fed to PV local controller ($S_{pv} = 1$), which represents MPPT operation. While ($S_{pv} = 0$), represents off-MPPT operation. The PV system is typically operated at MPPT. For efficient operation, fuel cell is typically operated in de-rated (off-MPPT) to have not much difference of efficiency. The fuel cell operating power reference signal is obtained using a reverse sigmoidal function of battery SoC (shown in Fig. 8), which is mathematically formulated as:

$$P^{*}_{fc} = P_{fc_{min}} + P_{fc_{max}} \cdot \frac{exp(\alpha(\beta - SoC)}{1 + exp(\alpha(\beta - SoC)} \tag{28}$$

Here α is saturation constant, β is the mid-value of SoC limits (typically chosen between 45 % – 55 %) and Pfcmax is the maximum possible power generation for considered P_{h_2} and $P0_2$ of the fuel cell. Based on power mismatch between the sources and load ($P_{pv} + P_{fc} - P_{load}$), the DC microgrid operation can be broadly classified into two different modes of operation, (1) Excess Generation Mode (EGM). (2) Deficit Generation Mode (DGM) as shown in Fig. 10.

3.1. Excess generation modes (EGM) ($P_{pv} + P_{fc} > P_{load}$) (modes: 1–5):

In EGM, the sum of average power from PV (P_{pv}) and fuel cell (P_{fc}) is

greater than P_{load}; under this, five operating modes are possible as shown in Fig. 10:

Mode 1 & 2 ($SoC \leq SoC_{min}$): In these modes, the objective of EMS is to increase *SoC* of the battery to bring it within limits. Hence, in both modes, the PV and fuel cell systems are always operated at MPP for a given solar irradiance, hydrogen and oxygen pressure, respectively. In mode 1, when $P_{h_2} \geq P_{h_2max}$, $P_{o_2} \geq P_{o_2max}$ i.e., P_{h2}, P_{o2} are held constant at maximum value, which means that the fuel cell output power is at maximum rating, and P_{h_2}, P_{o_2} difference is maintained at minimum value. The fuel cell continues to operate at the same point maintaining maximum power level till *SoC* increases beyond the lower limit. In mode 2, when $P_{h_2} \leq P_{h_2max}$, $P_{o_2} \leq P_{02max}$ the power of fuel cell (P_{fc}) is slightly increased as per reverse sigmoidal function given by Eq. (28) to operate it at maximum fuel cell power mode, hydrogen, and oxygen pressures P_{h_2max}, P_{o_2max} so as to ensure fast charging of BESS.

Mode 3 & 4 ($SoC \geq SoC_{max}$): In mode 3,the PV is operated in off-MPPT (derating) mode to ensure that BESS is either in floating mode or discharging mode. In mode 3, when $P_{pv} \geq P_{pv}$, i.e., the fuel cell generates derated power for supplying (P_{h_2}), with (P_{o_2}) minimum value; the EMS continues to maintain minimum power till battery *SoC* falls below SoC_{max}. In mode 4, when $P_{pv} \leq P_{load}$, PV operating in MPPT mode, fuel cell supplied the power generated is as per the reverse sigmoidal function (Eq. (28)), shown in Fig. 1 to ensure that battery operates either in floating mode or discharging mode.

Mode 5($SoC_{min} < SoC < SoC_{max}$): In mode 5, the PV is operated in MPPT mode while the fuel cell operates based on reverse sigmoidal function and charges the battery *SoC* to have a DC-link power balance and maintains DC link voltage nominally with reference to v_{dcref}.

3.2. Deficit generation modes (DGM) (Ppv + Pfc < Pload) (modes:6–9):

In DGM, the sum of powers from the sources PV (P_{pv}) and fuel cell (P_{fc}) is less than load demand (P_{load}). Under DGM, there can be four operating modes as shown in Fig. 10.

Mode 6 & 7 ($SoC \leq SoC_{min}$): The PV system and fuel cells are run at MPP in modes 6 and 7, respectively, for a given amount of solar irradiation and hydrogen and oxygen gas partial pressure. In mode 6, when $P_{h_2} \geq P_{h2max}$, $P_{o2} \geq P_{o_2max}$ i.e., P_{h_2}, P_{o_2} are maintained constant at maximum value; it signifies that fuel cell output power is at maximum rating, and P_{h_2}, P_{o_2} different is kept to a minimum value. Furthermore, if the load demand is not met using both PV and fuel cell and, optional loads are shed. This ensures that BESS doesn't discharge extensively. In mode 7, when $P_{h_2} \leq P_{h_2max}$, $P_{o_2} \leq P_{0_2max}$ the power of the fuel cell P_{fc} is slightly raised according to reverse sigmoidal function provided by Eq. (28) to operate it at maximum hydrogen, and oxygen pressures Ph_{2max}, Po_{2max} so as to ensure quick charging of BESS.

Mode 8 & 9: For modes 8 and 9, PV is operated at MPP in modes 8 and 9. In mode 8, battery $SoC \geq SoC_{max}$ or $SoC_{min} > SoC > SoC_{max}$; in this condition the fuel cell is supplied based on the reverse sigmoidal function as shown in Fig. 1, and the battery discharges up to above the lower limit. In mode 9, when $SoC_{min} > SoC > SoC_{max}$, PV operates as MPPT mode, battery *SoC* is maximum so it discharges up to above the minimum level of battery, and the fuel cell provides the load power based on reverse sigmoidal function as shown in Fig. 1; PV power, and battery power, are kept constant to maintain the load demand continuously.

Flowchart for modes of operation in PV, fuel cell and BESS system with proposed energy management strategy.

4. Stability analysis of proposed microgrid

The stability of the DC microgrid while regulating dc-link voltage is analyzed in this section. As the dc-link voltage controller remains the same in all control operating modes, stability is analyzed by considering DC-link voltage as system output and its controller is designed so as to have sufficient phase margin to the system open-loop transfer function. As BESS uses bidirectional boost converters, the transfer functions of the converter system are derived from the inductor current and capacitor voltage dynamics (Eqs. (29) and (30)), respectively.

$$L_{bat}.\frac{di_{Lbat}(t)}{dt} = v_{bat} - (1 - d_{bat})v_{cbat} \tag{29}$$

$$C_{bat}.\frac{dv_{cbat}(t)}{dt} = (1 - d_{bat})i_{lbat} - \left(-i_{load} + i_{pv} + i_{fc}\right) \tag{30}$$

The voltage control transfer functions [2,47], are generated using the state space averaging approach as follows:

$$G_{\Delta vdbat} = \frac{\Delta\widehat{v}_{bat}(s)}{\widehat{d}_{bat}(s)} = \frac{(1 - D_{bat})v_{dc} - L_{bat}I_{Lbat}s}{L_{bat}C_{bat}S^2 + \frac{L_{bat}i_{bat}}{V_{dc}}s + (1 - D_{bat})^2} \tag{31}$$

Moreover, the current control transfer function is computed as follows:

$$G_{i^*_{bat}dbat} = \frac{\widehat{i}_{i^*_{bat}}(s)}{\widehat{d}_{bat}(s)} = \frac{C_{obat}V_{dc}s + 2(1 - D_{bat})I_{Lbat}}{L_{bat}C_{bat}S^2 + \frac{L_{bat}i_{bat}}{V_{dc}}s + (1 - D_{bat})^2} \tag{32}$$

The simplified transfer function model with feedback control loop of BESS system is shown in Fig. 11. Here, it is noted that disturbance caused by exogenous inputs (i_{pv}, i_{fc}, and i_{load}) are eliminated using the feed forward loop [47] shown in Fig. 11. The battery current control loop is designed for a bandwidth of (5–10) less than the switching frequency, so that the controller action towards switching transients is avoided. The loop gain of the battery current control loop is given by:

$$L_{i_o,op} = PI_{i^*_{bat}}.GI_{i^*_{bat}}.H_1 \tag{33}$$

and the transfer function of a closed loop current control loop is:

$$L_{i_o,cl} = \frac{PI_{i^*_{bat}}.GI_{i^*_{bat}}}{1 + PI_{i^*_{bat}}.GI_{i^*_{bat}}.H_1} \tag{34}$$

The inner current controller PI gains are assigned using MATLAB/SISO toolbox. In the battery, inner current loop is designed with a bandwidth of 5000rad/s to ensure fast operation of battery during load transients and the phase margin is selected as 60° to provide sufficient damping and exhibit stable closed-loop operation. Fig. 12 depicts the bode diagram for such compensated and uncompensated battery current loop systems.

$$L_{v_o,op} = L_{i_o,cl}.Gv_{i^*_{bat}}.PI_{\Delta v} \tag{35}$$

The outer voltage controller is designed with a loop bandwidth of 500rad/s and phase margin of 60°. The Bode plot with and without compensator is shown in Fig. 12. The blue line represents the uncompensated system, whereas the red line represents the proposed accurate model [48,49].

5. Simulation studies

The efficacy of the proposed EMS was evaluated by simulating the DC microgrid system as shown in Fig. 1 in MATLAB/Simulink. The specifications of the PV systems, fuel cells, and battery along with their respective converter and control parameters used in simulation studies are detailed in Table. 2. The fuel cell generates a maximum output power ($P_{fcmax} = 220W$) for a maximum safe hydrogen pressure range ($P_{h_2} = 5.02bar$). The hydrogen pressure of the fuel cell cylinder is controlled through pressure control valve detailed in Sections 2, and 3. BESS is controlled using the cascaded control loop method for DC link voltage regulation. In this, the inner current controller is tuned using pole-zero placement approach and the outer voltage controller is tuned using the symmetrical optimal method. The upper and lower limits of battery *SoC* are considered as $SoC_{max} = 80\%$ and $SoC_{min} = 20\%$. and the EMS is designed to operate the battery within the limit of *SoC*. Further, for all test scenarios, the resistive loads are considered across the DC link and BESS local controller and it is designed to maintain DC link voltage

at a reference nominal value of v_{dcref}=100V.

5.1. Scenario 1 (SoC = 80 %):

In this scenario, the battery SoC is near its upper limit SoC_{max} as shown in Fig. 13(b). For these conditions, the performance of the proposed EMS is evaluated under varying load conditions. The initial load on the DC microgrid is $P_{load} = 280W$, and battery SoC is at 80% as shown in Fig. 13(a) and (b). As the battery SoC is at its upper limit, to avoid deep charging of the batteries, the proposed EMS, sends an $S_{pv} = 0$ signal to PV local control that makes PV operate in load follower mode for avoiding further charging of the battery. During this cycle, the hydrogen pressure is maintained at a minimum value based on reverse sigmoidal function output and the DC-link voltage is maintained at 100V by BESS controller. At time t = 3.5s, the total load P_{load} in DC microgrid is increased to 614W (Fig. 13(a)). As the load demand is increased, the battery starts discharging, and SoC falls below its upper limit. Based on this data, the proposed EMS provides PV MPPT on signal ($S_{pv} = 1$) to PV controller and enables MPPT operation as shown in Fig. 13(c). However, as the load $P_{load} = 614W$ is greater than PV MPP output power $P_{pv} = 430$, BESS continues to discharge by supplying $P_{bat} = 140W$. During this phase, the fuel cell is still supplying at minimum generation around $P_{fcmin} = 38W$ as shown in Fig. 13(e). At t = 9.5s, the load demand is reduced to 280W which results in the battery discharging till $SoC < SoC_{max}$. When BESS SoC reaches the maximum limit, the proposed EMS sends the off-MPPT signal to PV controller and makes PV operate in derated mode with output power condition $P_{pv} = P_{load}$ as shown in Fig. 13(c). Again, at t = 18s, the load demand increases to 380W, as SoC $\geq$ 80%; the PV continued to operate at Off-MPPT PV output equal to load demand. During this phase, the battery was operated in floating mode, and the fuel cell at minimum generation mode as shown in Fig. 13.

5.2. Scenario 2 (SoC = 20%):

In this scenario, the battery SoC is near its lower limit (SoC_{min}) as shown in Fig. 14(b). in these conditions, the performance of the proposed EMS is evaluated for varying load conditions. The initial load on the DC microgrid was $P_{load} > P_{pv} + P_{fc}$, and battery SoC was at 20% as shown in Fig. 14(a) and (b). The proposed EMS operated PV and fuel cell system in MPPT mode and fuel pressure is maintain in minimum mode is shown in Fig. 14(c), (d), (e), and the battery discharged to maintain the load demand while also avoiding deep discharging of the batteries. The optional load was shed at $t = 2s$ with net load being $P_{load} = 500W$. The battery started to charge. Further, the charge at $t = 8s$ led the load to being further reduced to $P_{load} = 400W$ battery at a faster rate. At $t = 14s$ the load increased and reached $P_{load} = 790W$, During this time, BESS discharged to maintain the load demand. At $t = 20.5s$, to avoid deep discharging, the load demand was again reduced as shown in Fig. 14.

5.3. Scenario 3 (SoC = 40 %, PV shaded condition):

In this scenario, load demand was maintained constant ($P_{load} = 670W$) as shown in Fig. 15(a). Initially, the battery SoC was considered at 40% within limits of SoC_{min} and SoC_{max} as shown in Fig. 15(b). During this phase, the PV was operated in MPPT mode, and the fuel cell power reference was obtained from reverse sigmoidal function of BESS SoC at $P_{fc}^* \approx 0.84P_{fcmax} = 193.2W$. BESS was operated in discharging mode with $P_{bat} = 51W$ to maintain the load demand as shown in Fig. 15(f). At $4s$, due to cloud shade, the PV output power was reduced to $P_{pv} = 360W$ as shown in Fig. 15(c), and fuel cell output was held at $P_{fc} = 193.5W$ as shown in Fig. 15(e). The additional load demand was met by the battery $P_{bat} = 120W$ with increased rate of discharge as shown in Fig. 15(b). At time $t = 9s$, the solar PV system irradiance was restored due to which the battery discharging rate reduced as depicted in Fig. 15(b).

6. Experimental results

The proposed EMS was validated using a hardware DC microgrid prototype model shown in Fig. 16. The schematic diagram of the hardware prototype is the same as in Fig. 1 with different ratings, which are tabulated in Table.2. A programmable PV simulator (Magna power electronics XR 250-6.0/200+PPPE+SL) was used to replace the PV system, the PEMFC (H-50 Horizon) with hydrogen a pressure (P_{h_2}) ranging from 1 to 5.02 (Bar) performed at 12V, 4.1A, and 40% efficiency, and two series-connected 12V/120Ah lead–acid batteries were used as sources, The local controllers of the individual source and the proposed EMS were implemented in dSPACE-DS1104 controller. The system was designed to maintain DC-link voltage at reference $V_{dcref} =$ 48V. Further, LEDs and incandescent bulbs were used as the DC loads in this system as shown in Fig. 16.

6.1. Scenario 1 (SoC = 80 %):

In this case, the performance of the proposed EMS was evaluated for varying load conditions while the battery SoC was near its upper limit with $SoC \approx 80\%$, as shown in Fig. 17. Initial $P_{load} \approx 80W$, $P_{pv} \approx 70W$, and $P_{fc} \approx 2W$. As $P_{load} > P_{pv} + P_{fc}$ and $SoC \approx 80\%$, the proposed EMS ensured that the MPPT operation for PV and fuel cell was in minimum power operation mode so that the battery discharged by supplying additional required power $P_{bat} \approx 8W$. At the time, t_1, the total load was P_{load} in DC microgrid and it decreased to $73W$(Fig. 17(a)). Even though the load decreased, $P_{load} > P_{pv} + P_{fc}$, the PV and fuel cell showed similar operation to that in pre-disturbance phase. However, the battery output power (P_{bat}) reduced to $1W$. At time t_2, the load was brought back to the initial value, which made all sources deliver the same output power as provided during the initial operation.

6.2. Scenario 2 (SoC = 80 %, PV shaded condition):

In this case, the load demand was held constant at ($P_{load} = 72W$) and PV was shaded from t_1 to t_2 as shown in Fig. 18(a). Initially, as $P_{load} > P_{pv} + P_{fc}$ and $SoC \approx 80\%$, the PV was operated in MPPT with output power $P_{pv} = 70W$; the fuel cell was operated at minimum power with $P_{fc} = 2W$ and the battery was in floating mode. At t_1, PV irradiance reduced which also decreased PV MPP to $P_{pv} = 60W$. As $P_{load} > P_{pv} + P_{fc}$ and $SoC \approx 80\%$, the battery supplied power of $P_{bat} = 10W$ to meet the load demand as shown in Fig. 18(b). At t_2, PV irradiance was restored to initial value due to which the battery was operated in floating mode.

6.3. Scenario 3 (SoC = 20 %):

Initially, $P_{load} \approx 82W$, $P_{pv} \approx 70W$, $P_{fc} \approx 50W$, and $SoC \approx 20\%$. The recommended EMS assured MPPT operations for PV, and fuel cell for maximum power operations to sustain load demand and charge the battery with a power rating of $P_{bat} = 38W$ are done by delivering additional power from fuel cell, as $P_{load} < P_{pv} + P_{fc}$ and $SoC \approx 21\%$. The load demand P_{load} in DC microgrid is reduced to $74W$ at time t_1, as illustrated in Fig. 19(a). Even though the load is reduced, PV is unable to meet the load requirement; thus, fuel cell inputs hydrogen to the maximum in supplying mode ($P_{fc} = 46W$) in combination with PV to meet the load demand, and charge the battery. At time t_2, the load is reset to power output as shown in Fig. 19(a), (b). as all sources generate the same power as initial operation.

6.4. Scenario 4 (SoC = 20 %, PV shaded condition):

As illustrated in Fig. 20 (a), the total load is kept constant at ($P_{load} = 82W$), and PV is shaded from t_1 to t_2.At first, because $P_{load} > P_{pv}$ and $SoC \approx 20\%$, the PV functioned in MPPT with a power output of $P_{pv} = 70W$, and the fuel cell was required to implement maximum output power mode with $P_{fc} = 50W$ to sustain power demands and recharge the

battery with an output power of $P_{fc} = 38W$. At t_1 instant, PV irradiation was lowered from $1000W/m^2$ to $700W/m^2$ which also lowered PV MPP to $P_{pv} = 60W$. Because of $P_{load} > P_{pv}$ and $SoC \approx 20\%$, a fuel cell with a power rating of $P_{fc} = 50W$ is required to fulfill the load demand and charge the battery, as shown Fig. 20 (a), and (b). The PV irradiation is returned to its initial value at t_2, allowing the battery to function in charging mode.

7. Comparative studies

In the current research, the PI control in MATLAB was configured with three input signals to the PV, FC, and battery. The efficacy of the proposed EMS is evaluated by comparing against the existing approaches developed in [50,51] and their comparison is tabulated in 1. The Strategy I and II are taken from [50,51], respectively. The isolate microgrid with PV, fuel cell, battery, and load power under two different operating conditions with battery SoC is maximum condition ($SoC_{min} =$ 80%) and minimum condition ($SoC_{min} = 20\%$)are considered for direct comparative analysis. In Table 1, an analytical comparison of existing techniques under these operating scenarios with load fluctuation is presented.

7.1. Energy management strategy comparison with method in [50]

Figs. 21 and 22 show the system operation with EMS in [50] and proposed strategy. In Fig. 22, initially, from $t = 0s$ to $2s$, $P_{load} = 700W$, and PV is operated at MPPT with $P_{pv} = 430W$, and fuel cell is supplying a power of $220W$ as load is greater than generation, the battery is in discharging mode. When the load is suddenly reduced to ($P_{load} = 600W$) at 2 s, the battery starts charging and goes beyond maximum SoCmax, i. e. 80%, leading to deep charging mode as shown in Fig. 22. At t=5s, the load is again increased to 700W, thus discharging battery. But with proposed EMS technique (shown in Fig. 22), at $t = 2s$, when the load demand falls to $P_{load} = 435W$, the total demand is less than the generation. This enables the charging of battery, however, battery SoC reached to 80%, the PV is automatically derated to 400W to avoid deep charging as shown in Fig. 22.

Table 1
Comparison of the proposed method against strategies [50,51].

Operation condition of DC microgrid and status of battery	Strategy-I [50]	Strategy-II [51]	Proposed EMS
Case.1: (SoC≥ 80%), under load variation	The PV controller is not designed to have derating mode. The battery can be over charged beyond safe limits under light load.	The PV controller is not designed to have derating mode. The battery can be over charged beyond safe limits under light load	The PV system can operate in derating mode as per requirement. The battery SoC is maintained at maximum limit, by derating PV.
Case.2: (20%< SoC<80%) under load variation	The fuel cell operates at constant power with no control over the Ph2 and Po2 pressure.	The fuel cell operates output power is varied by using addition control command from the controller. But no control over the Ph2 and Po2 pressure	The fuel cell power output is regulated using reverse sigmoidal function SoC, without loosing much of fuel cell efficiency
Case.3 (SoC≤ 20%), under load variation.	The PV system is operating in MPPT Mode The battery can be deeply discharged.	The PV system is operating MPPT Mode. The battery can be deeply discharged.	The PV system is operating in MPPT Mode. The battery SoC maintains (discharging, charging, and floating modes) by regulating the Ph2 and Po2 pressures within limitations.

Table 2
System parameters.

Parameters name	Simulation parameters	Experimental parameters
Specification for solar PV at STC (1000W/m^2, 25°C)		
Power at MPP (W)	54.69	70.2
Voltage at MPP (V)	16.88	31.2
Current at MPP (A)	3.24	2.25
Voltage at Voc (V)	21.1	39.36
Current at Isc (A)	3.6	2.5
No of cells	48	96
Each cell voltage(V)	0.44	0.41
Input capacitor Cin	500Mf	500μF
Output capacitor Cout	500μF	500μF
Inductor (Lpv)	4 mH,0.001×	4.5 mH
Specifications of PEMFC		
Rated power (W)	220	50
Number of cell	48	20
Purging at a voltage (V)	12	12
A (cm^2)	27	25
lμm	127	135
Jmax (mA/cm^2)	6.5	–
Ph2 pressure (bar)	1.00–5.21 (as per BESS SoC)	1.00–5.21
Temperature	343.15–353.15(K)	5◦ To 30◦
Purity of hydrogen	>99.995 % of dry Ph_2	>99.995 % of dry Ph_2
Shut down for over current (A)	12	12
Shut down for low voltage (V)	12	12
shut down at over temp	–	65◦
Time taken for start up	Immediate	<30s at ambi-ent temp
Reactants	Hydrogen and Air	Hydrogen and Air
Cooling	–	Air Cooling fan
Flow rate at max output power	–	840 ml/min
Efficiency	54 %	40 %
Input capacitor Cin	500Mf	500Mf
Output capacitor Cout	500 μF	500 μF
Inductor (Lfc)	4 mH, 0.001×	8.5 mH
Specification of BESS		
Battery choice	Lead–acid battery	Lead–acid battery
Rating in ampere hour	120 Ah	120 Ah
Nominal voltage	12 V	12 V
Charging rate	C/10	C/10
Capacitor (Cbat)	2000 μF	500 μF
Inductor (Lbat)	4.8 mH, 0.001×	7.2 mH

7.2. Advantages of proposed method

Typically, Fuzzy Logic Controller (FLC) [52], artificial neural network (ANN) algorithms [53], An adaptive neuro-fuzzy inference system (ANFIS) [54] methods are used for decision making problems. The major draw-back of these controllers is that it requires large numbers of training data and intense computational facilities. However, the implementation of rules based heuristic strategy is fairly simple and straight forward. In these approaches there is no requirement of large data set for training and does not need huge computational facilities and control actions are highly reliable. This makes it more feasible for real-world problems and can be implemented using already available computational facilities. Owing to these advantages, the author preferred the rule-based heuristic approach over any other artificial intelligent approaches However, these approaches are also having few challenges, especially; to frame the rules an expert knowledge is required.

8. Conclusions

In this paper, an effective EMS was proposed for standalone DC microgrid with PV/fuel cell/energy storage Systems. The EMS is developed for improved longevity of battery by maintaining the battery's SoC in an acceptable range and also for reduced hydrogen fuel intake in a fuel cell without compromising the system reliability. In normal operation, the PV system operates in MPPT mode to maximize the utilization of renewable energy. The fuel cell is operated as a function of battery SoC to avoid deep charging/discharging of the battery, which also improves the fuel cell efficiency. The battery bank is managed by EMS to ensure balanced power distribution sources and load, while regulating DC link voltage. The improved functionality of EMS manages the power flow between the fuel cell generating system and the storage battery under various operating conditions. The operating conditions are classified into 9 operational states based on BESS SoC, the system's total demand power, as well as optimal working points of distributed generators. These operational modes enable the de-rated operation of PV system under light load and high SoC conditions, MPPT operation of fuel cell under heavy load and low SoC. This avoids deep charging/discharging of batteries thereby improving their longevity, efficiency of the fuel cell under normal conditions, and increases reliability of the system under extreme conditions. The proposed EMS was validated in simulation and on hardware DC microgrid prototype under various battery SoC levels and loading conditions. According to the results, this method is able to regulate diverse distributed generation systems while maintaining power balance, as well as optimizing the DC microgrid system. In Further, the EMS can be slightly modified for effective operation of the system under transient conditions while limiting the battery discharge rate within acceptable limits using super-capacitor. Additionally, the application of the proposed EMS algorithm can be extended to microgrids with heterogeneous distributed generators.

CRediT authorship contribution statement

Conception and design of study: Ramesh Gugulothu, Dr. Nagu Bhookya, Dr. Deepak Pullaguram.

Aquisition of data: Ramesh Gugulothu

Analysis and/or interprestation of data: Ramesh Gugulothu, Dr. Deepak Pullaguram.

Drafting the manuscript: Ramesh Gugulothu, Dr. Nagu Bhookya, Dr. Deepak Pullaguram.

Revising the manuscript critically for important intellectual content: Ramesh Gugulothu, Dr. Nagu Bhookya, Dr. Deepak Pullaguram.

Approval of the version of the manuscript to be published: Ramesh Gugulothu, Dr. Nagu Bhookya, Dr. Deepak Pullaguram.

Declaration of competing interest

No.

Data availability

Data will be made available on request.

Acknowledgment

This work was partially supported by Science and Engineering Research Board (SERB), Govt. of India, under the head of (EEQ/2016/000814), and [SRG/2020/002557].

References

[1] H. Myneni, S.K. Ganjikunta, Energy management and control of single-stage grid-connected solar PV and BES system, IEEE Trans.Sustain.Energy 11 (3) (2020) 1739–1749.
[2] S. Kotra, M.K. Mishra, A supervisory power management system for a hybrid microgrid with HESS, IEEE Trans. Ind. Electron. 64 (5) (2017) 3640–3649.
[3] F. Nejabatkhah, Y.W. Li, Overview of power management strategies of hybrid AC/DC microgrid, IEEE Trans. Power Electron. 30 (12) (2015) 7072–7089.
[4] M. Marzband, E. Yousefnejad, A. Sumper, J.L. Domınguez-Garcıa, Real time experimental implementation of optimum energy management system in standalone Microgrid by using multi-layer ant colony optimization, Int.J.Electr. PowerEnergy Syst. 75 (2016) 265–274.
[5] A. Fathy, H. Rezk, A.M. Nassef, Robust hydrogen-consumption-minimization strategy based salp swarm algorithm for energy management of fuel cell/supercapacitor/batteries in highly fluctuated load condition, Renew. Energy 139 (2019) 147–160.
[6] A. Frances, R. Asensi, O. Garcia, R. Prieto, J. Uceda, Modeling electronic power converters in smart DC microgrids—an overview, IEEE Trans.Smart Grid 9 (6) (2018) 6274–6287.
[7] F.S. Al-Ismail, DC microgrid planning, operation, and control: a comprehensive review, IEEE Access 9 (2021) 36154–36172.
[8] V. Vega-Garita, M.F. Sofyan, N. Narayan, L. Ramirez-Elizondo, P. Bauer, Energy management system for the photovoltaic battery integrated module, Energies 11 (12) (2018).
[9] N. Karami, N. Moubayed, R. Outbib, Energy management for a PEMFC–PV hybrid system, Energy Convers. Manag. 82 (2014) 154–168.
[10] N. Eghtedarpour, E. Farjah, Distributed charge/discharge control of energy storages in a renewable-energybased DC micro-grid, IET Renew.Power Gener. 8 (1) (2014) 45–57.
[11] A.A.A. Alahmadi, Y. Belkhier, N. Ullah, et al., Hybrid wind/PV/battery energy management-based intelligent non-integer control for smart DC-microgrid of smart university, IEEE Access 9 (2021) 98948–98961.
[12] A. Garg, N.R. Tummuru, R. Oruganti, Implementation of energy management scenarios in a DC microgrid using DC bus signaling, IEEE Trans. Ind. Appl. 57 (5) (2021) 5306–5317.
[13] D. Lu, H. Fakham, T. Zhou, B. Francois, Application of Petri nets for the energy management of a photovoltaic based power station including storage units, Renew. Energy 35 (6) (2010) 1117–1124.
[14] D. Rekioua, Chapter 11 - energy management for PV installations, in: I. Yahyaoui (Ed.), Advances in Renewable Energies And Power Technologies, Elsevier, 2018, pp. 349–369.
[15] S. Taraft, D. Rekioua, D. Aouzellag, S. Bacha, A proposed strategy for power optimization of a wind energy conversion system connected to the grid, Energy Convers. Manag. 101 (2015) 489–502.
[16] M. Marzband, S.S. Ghazimirsaeid, H. Uppal, T. Fernando, A real-time evaluation of energy management systems for smart hybrid home microgrids, Electr. Power Syst. Res. 143 (2017) 624–633.
[17] N. Mebarki, T. Rekioua, Z. Mokrani, D. Rekioua, Supervisor control for stand-alone photovoltaic/hydrogen/ battery bank system to supply energy to an electric vehicle, Int. J. Hydrog. Energy 40 (39) (2015) 13777–13788.
[18] N. Bahri, W.O. Amor, Intelligent power supply management of an autonomous hybrid energy generator, Int. J. Sustain. Eng. 12 (5) (2019) 312–332.
[19] H. Hassani, F. Zaouche, D. Rekioua, S. Belaid, T. Rekioua, S. Bacha, Feasibility of a standalone photovoltaic/ battery system with hydrogen production, J.Energy Storage 31 (2020), 101644.
[20] M.F. Elmorshedy, M. Elkadeem, K.M. Kotb, I.B. Taha, D. Mazzeo, Optimal design and energy management of an isolated fully renewable energy system integrating batteries and supercapacitors, Energy Convers. Manag. 245 (2021), 114584.
[21] C. Serir, D. Rekioua, N. Mezzai, S. Bacha, Supervisor control and optimization of multi-sources pumping system with battery storage, Int. J. Hydrog. Energy 41 (45) (2016) 20974–20986.
[22] L. Valverde, F. Rosa, A. del Real, A. Arce, C. Bordons, Modeling, simulation and experimental set-up of a renewable hydrogen-based domestic microgrid, Int. J. Hydrog. Energy 38 (27) (2013) 11672–11684.
[23] P. Thounthong, V. Chunkag, P. Sethakul, S. Sikkabut, S. Pierfederici, B. Davat, Energy management of fuel cell/solar cell/supercapacitor hybrid power source, J. Power Sources 196 (1) (2011) 313–324.
[24] A. Brka, G. Kothapalli, Y.M. Al-Abdeli, Predictive power management strategies for stand-alone hydrogen systems: lab-scale validation, Int. J. Hydrog. Energy 40 (32) (2015) 9907–9916.
[25] E.G. Shehata, M.S. Gaber, K.A. Ahmed, G.M. Salama, Implementation of an energy management algorithm in DC MGs using multi-agent system, Int.Trans.Electr. Energy Syst. 29 (4) (2019), e2790.
[26] A novel control strategy and power management of hybrid PV/FC/SC/battery renewable power system based grid-connected microgrid, Sustain. Cities Soc. 44 (2019) 830–843.
[27] Amin, R.T. Bambang, A.S. Rohman, C.J. Dronkers, R. Ortega, A. Sasongko, Energy management of fuel cell/battery/supercapacitor hybrid power sources using model predictive control, IEEE Trans. Ind. Informa. 10 (4) (2014) 1992–2002.
[28] L. Valverde, C. Bordons, F. Rosa, Integration of fuel cell technologies in renewable-energy-based microgrids optimizing operational costs and durability, IEEE Trans. Ind. Electron. 63 (1) (2016) 167–177.
[29] N. Bizon, M. Radut, M. Oproescu, Energy control strategies for the fuel cell hybrid power source under unknown load profile, Energy 86 (2015) 31–41.

[30] J. Han, J.F. Charpentier, T. Tang, An energy management system of a fuel cell/battery hybrid boat, Energies 7 (5) (2014) 2799–2820.
[31] S. Li, C. Gu, P. Zhao, S. Cheng, Adaptive energy management for hybrid power system considering fuel economy and battery longevity, Energy Convers. Manag. 235 (2021), 114004.
[32] M.G. Villalva, J.R. Gazoli, E.R. Filho, Comprehensive approach to modeling and simulation of photovoltaic arrays, IEEE Trans. Power Electron. 24 (5) (2009) 1198–1208.
[33] Z. Zhao, R. Cheng, B. Yan, et al., A dynamic particles MPPT method for photovoltaic systems under partial shading conditions, Energy Convers. Manag. 220 (2020), 113070.
[34] N. Mezzai, D. Rekioua, T. Rekioua, A. Mohammedi, K. Idjdarane, S. Bacha, Modeling of hybrid photovoltaic/wind/fuel cells power system, Int. J. Hydrog. Energy 39 (27) (2014) 15158–15168.
[35] S. Aissou, D. Rekioua, N. Mezzai, T. Rekioua, S. Bacha, Modeling and control of hybrid photovoltaic wind power system with battery storage, Energy Convers. Manag. 89 (2015) 615–625.
[36] N. Femia, G. Petrone, G. Spagnuolo, M. Vitelli, Optimization of perturb and observe maximum power point tracking method, IEEE Trans. Power Electron. 20 (4) (2005) 963–973.
[37] Services ET, Fuel Cell Handbook, Solid State Energy Conversion Alliance, USA, 2002.
[38] C. Wang, M. Nehrir, S. Shaw, Dynamic models and model validation for PEM fuel cells using electrical circuits, IEEE Trans.Energy Convers. 20 (2) (2005) 442–451.
[39] Z. Ural Bayrak, M. Gencoglu, B. Gumus, in: Dynamic simulation of a PEM fuel cell system, 2007, pp. 13–15.
[40] W. Saeed, G. Warkozek, Modeling and analysis of renewable PEM fuel cell system, Energy Procedia 74 (2015) 87–101.
[41] I. Papagiannakis, Studying And Improving the Efficiency of Water Electrolysis Using a Proton Exchange Membrane Electrolyser, 2005.
[42] R. Gugulothu, B. Nagu, D. Pullaguram, A computationally efficient jaya optimization for fuel cell maximum power tracking, Energy Sources, Part A 44 (1) (2022) 1541–1565.
[43] J. Correa, F. Farret, L. Canha, M. Simoes, An electrochemical-based fuel-cell model suitable for electrical engineering automation approach, IEEE Trans. Ind. Electron. 51 (5) (2004) 1103–1112.
[44] K.W. Harrison RR, G. Martin, Hydrogen production: fundamentals and case study summaries, in: National Renewable Energy Laboratory, 8th World Hydrogen Energy Conference Essen, Germany NREL/CP-550- 47302, 2010. CP: 550-47302.
[45] J. Appleby, F. Foulkes, Fuel Cell Handbook, Texas AM University, Van Nostrand Reinhold, New York, 1989 (out of print) republished by Krieger Publishing Co., Melbourne.
[46] W. Winkler, Thermodynamics, in: S.C. Singhal, K. Kendall (Eds.), High Temperature Solid Oxide Fuel Cells: Fundamentals, Design And Applications, Elsevier Ltd., Oxford, UK, 2003, pp. 53–82.
[47] W. Erickson Robert, Maksimovic Dragan, Fundamentals of Power Electronics, Springer, 2020.
[48] C.R.P.S. Arunkumar, Supercapacitor-based Transient Power Supply for DC Microgrid Applications 21(5), Springer part of Springer Nature 2021, 2021.
[49] Y. Zhang, Li Y. Wei, Energy management strategy for supercapacitor in droop-controlled DC microgrid using virtual impedance, IEEE Trans. Power Electron. 32 (4) (2017) 2704–2716.
[50] A. Kamel, H. Rezk, N. Shehata, J. Thomas, Energy management of a DC microgrid composed of photovoltaic/ fuel cell/battery/supercapacitor systems, Batteries 5 (3) (2019).
[51] Y. Han, W. Chen, Q. Li, Energy management strategy based on multiple operating states for a photovoltaic/fuel cell/energy storage DC microgrid, Energies 10 (1) (2017).
[52] N.E. Benchouia, A. Derghal, B. Mahmah, B. Madi, L. Khochemane, Aoul E. Hadjadj, An adaptive fuzzy logic controller (AFLC) for PEMFC fuel cell, Int. J. Hydrog. Energy 40 (39) (2015) 13806–13819.
[53] N. Mallick, V. Mukherjee, Maximum power point tracking supported proton exchange membrane fuel cell based intelligent dynamic voltage restorer, Int. J. Hydrog. Energy 45 (53) (2020) 29271–29287.
[54] K. Reddy, D.S. Natarajan, ANFIS-MPPT control algorithm for a PEMFC system used in electric vehicle applications, Int. J. Hydrog. Energy 44 (2019).